J. Fluid Mech. (1979), *vol.* 94, *part* 4, *pp.* 649–672
Printed in Great Britain

Experimental investigation of flow and heating in a resonance tube

By VIRENDRA SAROHIA AND LLOYD H. BACK
Jet Propulsion Laboratory, California Institute of Technology, Pasadena, California 91103

(Received 3 March 1978)

Experiments have been performed to determine the basic mechanism of heating in resonance tubes of square section with constant area excited by underexpanded jet flows. The jet flow between the nozzle exit and the tube inlet plays a key role in the performance of a resonance tube. A detailed and systematic investigation of the unsteady complex shock structure in this part of the flow region has led to a better understanding of the fundamental mechanisms associated with the gas heating in such tubes. A study of the effects of tube location in relation to free-jet shock location (without the presence of the resonance tube) has shed further light on the underlying mechanism of sustained oscillations of the flow in a resonance tube.

1. Introduction

Since Hartmann's (1931) discovery of the resonance tube phenomenon, many researchers have investigated certain aspects of the fluid dynamics associated with this device. It has long been known that, for a wide range of resonance tube configurations such as length of the tube, spacing between the nozzle exit and the tube inlet, nozzle-to-tube-diameter ratio, length of the tube, and nozzle flow conditions, intense and very rapid heating of the gas near the endwall can be obtained. Heating can occur when either subsonic or supersonic jet flows impinge on the open end of the tube. The characteristics of the rapid, intense heating of the endwall tube gas have led investigators to consider the application of resonance tubes as a possible method of igniting a rocket engine (e.g. Stabinsky 1973; and Marchese 1974). Resonance tube flows are also of interest because the intense heating of the tube gas is accompanied by generation of high-intensity ultrasonic waves (Rozenberg 1969) which can be employed for ultrasonic drying and for fog dissipation (Brun & Boucher 1957).

Hartmann (1931) observed that high-intensity sound waves are generated when an air-jet oscillator such as the resonance tube is placed in the region where the pressure in the jet is rising, i.e. the so-called 'zones of instability'. This high-intensity ultrasonic sound generation by the air-jet generator when placed in these zones of jet instabilities showed a large amplitude of almost normal shock wave oscillation in front of the air-jet generator inlet (cf. Hartmann 1931, plate IX). The frequency of this shock wave oscillation in the 'zone of instability' decreased with increasing distance between the nozzle exit and the inlet of the air-jet generator. These large-amplitude oscillations of the shock wave in the jet flow disappear and reappear with varying spacing between the nozzle exit and the tube inlet. However, no detailed and systematic investigation of this mode of air-jet generator on heating of the tube gas has been undertaken.

0022-1120/79/4223-7220 $02.00

Sprenger (1954) studied at length the effects that nozzle-tube spacing, nozzle stagnation pressure, and length of the tube have on the endwall tube temperature. For a given resonance tube and jet flow, many peaks in the endwall tube temperature about as high as 750 °K were observed. It was also noticed that, for a given resonance tube, large variations in endwall gas temperature were noticed when slight changes in nozzle pressure ratio or spacing between the nozzle exit and the tube inlet were made. However, no detailed study was undertaken to investigate the resonance tube flows that produced the drastic changes in the endwall temperature.

Previous work on the fluid dynamics of resonance tubes has been mainly experimental. Most of the investigators in the past (Brocher, Maresca & Bournay 1970; Brocher & Maresca 1973; Thompson 1960) concentrated on the particular mode of resonance tube operation in which the jet flow between the nozzle exit and tube inlet is periodically swallowed by the tube. As compared to Hartmann's resonance tube operation with tube inlet located in the spatial zones of instability, in this periodic jet swallowing mode of operation (referred to in this paper as the jet regurgitant mode), quite unique, periodic shock wave structure in the jet flow results (Thompson 1960). Under certain conditions of flow and tube configuration, in this periodic swallowing mode of resonance tube operation, shock waves are formed inside the tube (Brocher *et al.* 1970; Lloyd 1958). The frequency of shock wave oscillations in the tube is at the tube fundamental frequency given by $f \simeq a/4L$, where a is the average acoustic speed inside the tube and L is the tube length. Most of the heating in the tube is caused by the dissipation processes, i.e. increase in the entropy, through the shock waves.

Attempts have been made to predict the maximum attainable gas temperatures in resonance tubes in the jet regurgitant mode of operation (Wilson & Resler 1959; Shapiro 1960). The predicted temperatures in these investigations are very high compared to the measured temperatures. It is felt that the detailed study of the tube flow in this mode of operation will shed more light on the various heat loss mechanisms (other than wall conduction which is thought to be the main source of heat loss from the tube) which limit the attainable temperatures in the tube. It is strongly felt that a detailed investigation of wave speed and flow inside the tube during various phases of jet regurgitant mode cycle is needed. These experimental observations, along with pressure and temperature measurements in this mode of operation, will be of valuable assistance in predicting the resonance tube performance accurately.

Although there is a fair amount of knowledge about the regurgitant mode of the resonance tube, little is known about the thermal effects for the mode of operation in which a normal shock wave stands in the resonance tube jet flow and oscillates at high frequency (e.g. Mørch 1964). Frequency of shock oscillation in the jet flow in this mode of operation strongly depends upon spacing between nozzle exit and tube inlet, nozzle pressure ratio, etc., and is virtually independent of the length of the resonance tube.

In the present study, the effects of nozzle flow and of tube configuration on tube gas heating for various resonance tube modes of operation were investigated. The jet flow between the nozzle exit and tube inlet plays a key role in the resonance tube performance. An investigation of the unsteady complex shock structure in this part of the resonance tube flow has led to a better understanding of the fundamental mechanism associated with gas heating in such tubes. The structure of the jet flow located between the nozzle exit and tube inlet was correlated with the free-jet structure i.e. without the presence of the tube. Of particular interest is the mode of operation in which rapid, intense heating of the tube gas occurs.

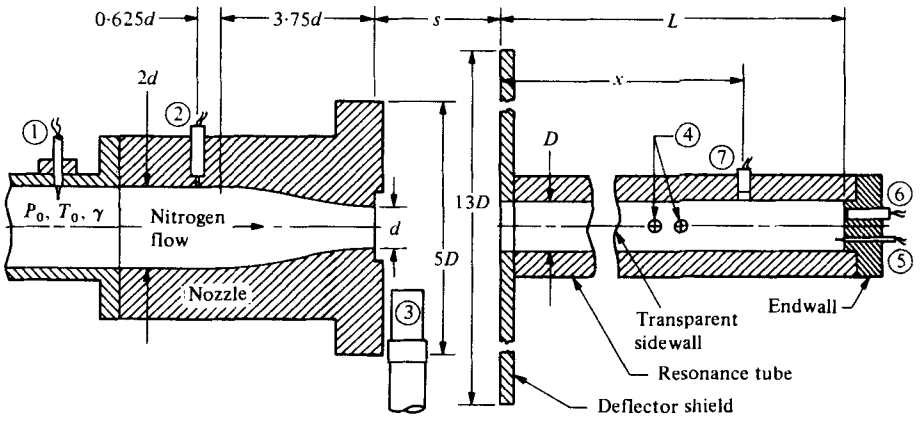

FIGURE 1. Resonance tube apparatus and instrumentation. 1, Total temperature thermocouple (22 gauge chromel–alumel wire). 2, Pressure transducer. 3, Microphone trigger for oscilloscope recording. 4, Laser beam pair for wave velocity measurement (variable spacing and axial location). 5, Endwall gas-temperature thermocouple (40 gauge chromel–alumel wire). 6, Endwall pressure transducer. 7, Sidewall pressure transducer. $d = 2{\cdot}03$ cm; $1{\cdot}0 \leqslant s/d \leqslant 6$; $D = 1{\cdot}25d$; $L/D = 3, 7, 14$.

2. Experimental apparatus, instrumentation, and measuring techniques

The various modes of resonance tube operation were investigated using the apparatus shown in figure 1. The tubes were square in cross-section, having a width of 2·54 cm and lengths 7·6, 17·8, and 35·6 cm. The sidewalls of the resonance tubes were lucite so that wave speeds could be determined and the tube flow could be visualized. The endwall and the upper and lower tube walls were made of micarta. For any given test, the centre-line of the nozzle was aligned with that of the tube inlet. Compressed nitrogen at ambient stagnation temperature was expanded through the convergent nozzle, which had an exit diameter $d = 2{\cdot}03$ cm. The ratio of the width of the square cross-sectional tube to nozzle exit diameter $D/d = 1{\cdot}25$ was kept constant throughout these experiments. The nozzle pressure ratio $R = P_0/P_\infty$, where P_0 is nozzle stagnation pressure and P_∞ the ambient pressure, could be varied up to a value of approximately 8·2. The spacing between the tube entrance and the nozzle exit was adjusted at values of $s/d = 1{\cdot}0$, 1·5, 1·75, 2·0, 3·0, 3·5, and 4·0. A deflector shield which had an outer diameter of 33 cm was placed at the entrance of the resonance tube to prevent the nitrogen from flowing over the outside of the tube. This allowed flow visualization as well as wave speed measurements inside the tube without the disturbances from the flow around the tube.

Both endwall gas temperature and endwall pressure traces as a function of time were obtained at different nozzle pressure ratios and various spacings between the tube inlet and the nozzle exit and for different tube lengths. The gas temperature was measured with 40-gauge chromel–alumel wire of 0·007 cm diameter. The response time of this thermocouple in the present experiments was estimated to be approximately 50 ms or less. The output of the thermocouple was recorded on an oscilloscope. A microphone located close to the jet flow was used to trigger the oscilloscope.

Kistler pressure transducers flush-mounted on the endwall were used to obtain fluctuating pressure inside the tube. These transducers had a resolution of 0·014 N/cm^2

(0·02 psi) with a rise time of 2 μs. The frequency response of the pressure transducers was from 2 to 40000 Hz. The output of the transducers drifted as the temperature increased; therefore, these transducers could only be used for determining the pressure jumps in a trace. To determine absolute levels of the pressures inside the tube in a cycle, pressure transducers were installed flush with the sidewall. The absolute levels of pressure inside the resonance tube were indirectly determined by studying the pressure jump across the incident and reflected shock waves close to the endwall. In addition, it was necessary to know the wave speed, which was determined both by a laser–schlieren technique and by observing simultaneously the pressures at two locations a known distance apart on the sidewall.

The laser–schlieren technique employed to measure wave velocity inside the square tubes used two parallel laser beams, a known distance apart, which were projected through the lucite walls and sensed by two photomultipliers. As the wave passed across one laser beam, the emerging beam was deflected by an angle proportional to the density gradient across the wave. A schlieren system was set up by intercepting this part of the deflected light. By cross-correlating data from the two beams, the incident, reflected, and contact surface velocities in the tube were determined. The beams were moved along the length of the tube to measure the velocities at different axial locations.

Instant spark shadowgraphs, as well as motion pictures of the resonance tube flows, were taken using an electronic strobotac. The flash duration of this strobotac was less than 3 μs, during which time the resonance tube flow was photographed. This duration was short enough to 'freeze' the flow field. Instant shock structure of a free-jet flow without the tube installed, as well as of the flow with the resonance tube in place, was obtained at various nozzle pressure ratios R and for different resonance tube configurations. By adjusting the flashing rate of the strobotac to an integral multiple of the speed of the jet shock-wave oscillation frequency, a stationary shock structure was observed. The flashing rate could be varied between 110 and 25000 flashes/min. Also, by flashing near to, but not synchronized with, the shock-wave oscillation frequency, a slow-motion replica of the actual motion was observed. This information was used to arrange the random still shadowgraphs of the jet flow between the nozzle exit and the tube inlet in a sequence of events within a cycle of tube operation.

During the course of this investigation, it was found that leaks have a severe effect on tube performance. Therefore, before any measurements were made, the tube was pressurized and checked for leaks.

3. Various modes of resonance tube operation

On the basis of the present systematic investigation over a wide range of nozzle pressure ratios R, spacing ratios s/d (see figure 1), and resonance tube lengths L, and past investigations (e.g. Hartmann 1931; Brocher *et al.* 1970; and Thompson 1960), the resonance tube flows can be divided into three modes of operation:

(1) Jet instability mode;
(2) Jet regurgitant mode;
(3) Jet screech mode.

3.1. *Jet instability mode*

This mode of resonance tube operation occurred only for a subsonic jet, i.e. $R < 1{\cdot}9$ over a wide range of spacing s/d. Spark shadowgraphs of the jet flow, as will be discussed later, indicated the formation of large, periodic vortices at the nozzle exit. These toroidal vortices in the jet flow grew in size as they convected downstream and resulted in weak compression waves inside the tube. These waves had a frequency equal to that of the vortex-shedding frequency. The oscillation frequency of the jet flow in this mode was found to occur in a narrow range of non-dimensional frequency parameter $fd/U_j \simeq 0{\cdot}3$ to $0{\cdot}4$, where U_j is the mean velocity at the nozzle exit. For certain flow conditions and tube configurations, this oscillation frequency was superimposed on the fundamental tube resonance frequency $f \simeq a/4L$. The weak shock waves formed in the resonance tube in this mode of operation did not result in any significant increase in the gas temperature measured at the endwall. As the nozzle pressure ratio R was increased above $1{\cdot}9$, a periodic shock structure appeared in the jet flow between nozzle exit and the tube inlet. Depending upon the spacing s/d, the tube flow switched either to the regurgitant mode or to the screech mode of operation. These two modes are discussed below.

3.2. *Jet regurgitant mode*

The jet regurgitant mode, as has been observed by other investigators (e.g. Thompson 1960), consists of periodic swallowing and discharging of the jet flow by the tube at the fundamental tube resonance frequency. From the present spark shadowgraph pictures and from endwall pressure and temperature measurements, it has been concluded that:

(i) The first part of the regurgitant mode of tube operation was the inflow phase of the tube. Most of the jet flow entered the tube. Depending on the nozzle pressure ratio R, either a diamond cell shock structure or a barrel shock was present in front of the inlet of the tube. The jet shock wave structure in this phase of the cycle depended only on the initial condition: nozzle diameter, nozzle pressure ratio R, etc. That is, the jet flow between the nozzle exit and tube inlet behaved as if the tube was not present in the jet flow. The portion of the jet flow that entered the tube caused the formation of compression waves. These compression waves then travelled toward the endwall. Coalescence of the compression wave train to a shock wave depended on tube length. In one case an almost normal shock wave was formed or else there was a shock wave which was followed by a train of compression waves. The waves were reflected from the endwall as a shock wave or a shock wave followed by a train of compression waves. The strengthening of the shock wave by coalescence of compression waves continued until this reflected wave front reached the inlet of the tube. From there the compression wave front resulted in the formation of a strong expansion wave front which travelled into the tube. The flow then suddenly switched to a transition phase followed by the outflow phase of its cycle in the regurgitant mode.

(ii) The presence of the expansion waves and reduced pressure behind the wave front caused the gas in the tube to flow outwards. The transition from inflow to the outflow phase resulted in a collision of the nozzle-jet and the tube-jet flows, thereby forming an interface. As the tube-jet flow gained in strength, the plane of the interface moved toward the nozzle.

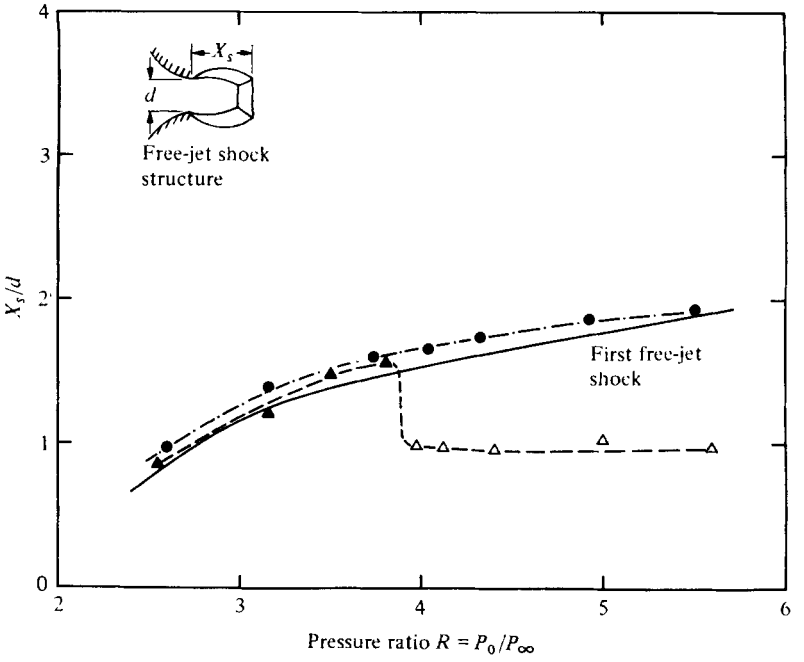

FIGURE 2. Effect of nozzle pressure ratio R on shock wave location during 35·6 cm tube jet-filling phase in regurgitant and screech modes of operation. ▲, s/d = 1·5, jet regurgitant; △, s/d = 1·5, jet screech; ●, s/d = 3·0, jet regurgitant.

(iii) At the end of the transition period between the inflow and the outflow phases, the two opposing jet flows remained in this stage almost the same period of time as the inflow phase of the jet regurgitant mode. The outflow phase of the tube was completed as the expansion fan approached the tube inlet after reflexion from the endwall. This resulted in a sudden weakening of the tube-jet flow.

(iv) As the tube flow weakened, the interface quickly moved toward the inlet of the tube. Then the nozzle flow again reverted back to the inflow phase of the regurgitant mode of resonance tube operation, and thus one cycle of operation was completed at the tube fundamental frequency. As compared to transition from tube inflow to outflow, the time required in switching from the outflow phase to the inflow phase was relatively short.

The actual duration of the various phases of a typical resonance tube cycle was not measured. Thompson (1960) studied at length the time required to complete these phases of a cycle of jet regurgitant mode. The structure of the flow inside the tube during the regurgitant mode of resonance tube operation will be discussed in § 4.

3.3. *Jet screech mode*

As previously discussed, in the inflow phase of the jet regurgitant mode, the jet flow between the nozzle exit and the tube inlet behaved like a free jet, i.e. without the presence of the tube in the jet flow. The jet flow went through this part of the regurgitant mode cycle if the spacing s/d was greater that the free-jet shock location $(X_s/d)_{\text{free jet}}$ (see legend to figure 2). But, as the pressure was increased for a given tube spacing, $(X_s/d)_{\text{free jet}}$ increased, until a nozzle pressure ratio R was reached for

which $s/d = (X_s/d)_{\text{free jet}}$. The present experiments indicated that the jet flow between the nozzle and the tube mouth then switched suddenly from the jet regurgitant mode and resulted in the formation of an almost normal shock in front of the inlet of the resonance tube. This shock oscillated at high frequency. The presence of this oscillating, almost normal, shock wave (frequency as high as 20 kHz in this study) in front of the resonance tube inlet has led us to call this the jet screech mode of resonance tube operation. The strength and location of this shock as well as its oscillation frequency depended upon the spacing s/d, nozzle pressure ratio R, etc. The boundary between the screech and regurgitant modes of operation is given by $s/d = (X_s/d)_{\text{free jet}}$; i.e. the spacing is equal to the location of the shock in the free jet. For $(X_s/d)_{\text{free jet}} \gtrsim s/d$, the resonance tube operated in the screech mode and the jet flow was prevented from going into the filling phase (i.e. the steady inflow phase as discussed previously under the jet regurgitant mode).

The experimental results that support these conclusions are shown in figure 2. This figure indicates the shock location X_s/d, in the jet flow between the nozzle exit and the tube inlet for the 35·6 cm resonance tube with spacing $s/d = 1{\cdot}5$ and 3·0 at different nozzle pressure ratios R. The location of the free-jet shock, $(X_s/d)_{\text{free jet}}$, as a function of R is also indicated. The experimental points in the regurgitant mode in figure 2 show the position of the shock X_s/d, in the filling or inflow phase. For the jet screech mode, figure 2 indicates the mean position of the oscillating normal shock in front of the inlet of the resonance tube.

As expected, up to a spacing $s/d = 1{\cdot}5$, the experimental points for the shock location X_s/d, in the inflow phase of the regurgitant mode, lie on the free-jet shock location $(X_s/d)_{\text{free jet}}$. Therefore, the jet flow in the filling phase of the jet regurgitant mode of operation behaves as if the tube were not present in the flow. This behaviour of the jet continued until a pressure ratio $R = 3{\cdot}9$ was reached, at which the flow between the nozzle exit and the tube inlet switched to the jet screech mode. At this pressure, the free-jet shock location $(X_s/d)_{\text{free jet}}$ was approximately equal to the tube spacing s/d. Now, a normal shock appeared in front of the tube inlet all the time and oscillated about its mean position. As the pressure was increased further, the spacing s/d was always less than the free-jet shock location $(X_s/d)_{\text{free jet}}$. Therefore, the jet flow remained in the jet screech mode.

Also in figure 2 are shown the experimental points in the filling phase for the 35·6 cm tube with spacing $s/d = 3{\cdot}0$. Over the range of pressure investigated, the flow remained in the jet regurgitant mode. The experimental points of shock wave location in the inflow phase X_s/d lie very close to the free-jet location $(X_s/d)_{\text{free jet}}$, further confirming the conclusions drawn above.

The experimental results for different tube lengths indicating the demarcation line between jet regurgitant and screech modes are shown in figure 3. The results of the first and second free shock location $(X_s/d)_{\text{free jet}}$ are compared with those obtained by Westley & Woolley (1968). As is clear from figure 3, the present results indicated that the shock waves were located farther downstream of the nozzle exit when compared to the data of Westley & Woolley for a given pressure. The experimental results reported herein were derived from free-jet shadowgraphs. Therefore, one cannot expect exact agreement. Along the first free-jet shock locations are indicated the spacings s/d at which the jet flow between the nozzle and the resonance tube inlet switched between jet screech and jet regurgitant modes. The experimental points for the various

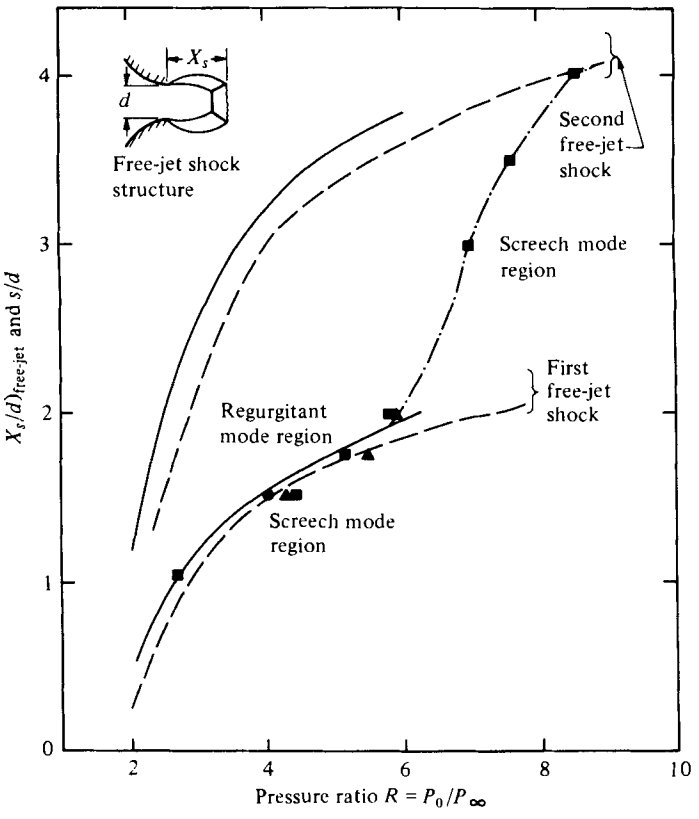

FIGURE 3. Regions of resonant tube operation. Experiment points when tube switched between screech and regurgitant modes, s/d curves: ●, 35·6 cm tube; ▲, 17·8 cm tube; ■, 7·6 cm tube. Free-jet shock location, $(X_s/d)_{\text{free jet}}$ curves: ——, present experiments; – – –, Westley & Woolley (1968).

tube lengths lie very close to the first-free jet shock location, confirming the fact that the jet-flow switch between the regurgitant and screech mode occurred at a pressure for which the spacing s/d was approximately equal to the corresponding first free-jet shock location; i.e. $s/d = (X_s/d)_{\text{free jet}}$.

As the pressure ratio R was increased beyond 6, the experimental points when the switch between jet regurgitant and screech modes occurred did not follow the free-jet shock location $(X_s/d)_{\text{free jet}}$ (figure 3). In fact, the switch to the screech mode occurred at larger tube spacing s/d until the tube came into the influence of the second free-jet shock at a pressure ratio $R \simeq 8{\cdot}4$. In figure 3, these points have been joined by a dotted line which separates the jet regurgitant and screech modes. It should be noted that the various regions of resonance tube operation were independent of the length of the tube.

It was also observed that in the jet screech mode the almost normal shock wave in front of the tube inlet oscillated in various bands of frequencies depending upon the pressure ratio R and the spacing s/d. The effects of various stages of shock wave oscillation in the jet screech mode are discussed in subsequent sections. Also note that the various modes of resonance tube flows discussed above pertain to the interaction

of the first free-jet shock cell structure with the tube inlet. Similar results were observed when the tube was placed in other shock cells.

4. Visualization of resonance tube flows

A critical examination of the spark shadowgraph pictures of resonance tube flows under various flow conditions, as discussed below, provided insight on the mechanism of gas heating in resonance tubes.

4.1. *Free-jet flow visualization*

Free-jet flows were observed over a range of nozzle pressures at which the resonance tubes were studied. As indicated above, the behaviour of the free jet is closely related to resonance tube operation in various modes. The effect of tube location in the resonance tube system with respect to that of the free-jet shock is shown in figures 2 and 3. This information is useful in the design of a resonance tube system for a particular mode of operation.

In this study, both subsonic and underexpanded supersonic jet flows from a convergent nozzle were examined. Typical shadowgraphs of the free jet at various nozzle pressure ratios are shown in figure 4 (plate 1). For nozzle pressure ratios $R \lesssim 1{\cdot}9$, the jet was subsonic. For $R > 1{\cdot}9$, the flow was underexpanded and resulted in the formation of shock waves downstream from the nozzle exit. Within the nozzle pressure ratios $1{\cdot}9 < R < 3{\cdot}4$, the diamond shock structure was observed. For pressures $R > 3{\cdot}4$, the 'Mach disc' appeared across the jet axis. The strength of this normal Mach disc as well as its distance from the nozzle exit increased as the nozzle pressure ratio R was increased.

Large spinning lateral motion of the whole jet flow was observed in the range of pressure ratios $1{\cdot}9 < R < 3{\cdot}4$ when the diamond shock structure was observed. This periodic lateral motion of the whole jet seems to result in large jet spreading rates. A large growth rate of the free jet is seen in the instantaneous shadowgraph in figure 4 at a nozzle pressure ratio $R = 2{\cdot}87$.

4.2. *Shadowgraphs of resonance tube flows at different nozzle pressures*

(i) *Flow between nozzle exit and tube inlet at* $s/d = 3$. Sequences of instant spark shadowgraphs for the 35·6 cm resonance tube with spacing $s/d = 3$, indicating the jet flow between nozzle exit and tube inlet at various pressures, are shown in figure 5 (plates 2, 3 and 4). The flow in these pictures was from left to right. The shadow at the top left in figure 5(*a*) was that of the triggering microphone which was placed in such a way as not to disturb the jet flow. These instantaneous shadowgraph pictures in figure 5 were taken at random and have been put in order of increasing time duration of a typical resonance tube cycle from top downwards. The corresponding endwall pressure traces, which are discussed in § 5, are indicated in figure 9.

In this section, the various resonance tube modes will be referred to as first or second mode of tube operation, depending upon the interaction of the resonance tube inlet with the first or second free-jet shock cells, respectively.

The jet flow in shadowgraph A of figure 5(*a*) at a pressure ratio $R = 1{\cdot}23$ with spacing $s/d = 3$ was subsonic. Toroidal vortices shed from the nozzle exit can be seen

in these pictures. These vortices grew in size as they propagated toward the resonance tube. The frequency of the vortices scaled as $fd/U_j \simeq 0{\cdot}3$ to $0{\cdot}4$. On interaction with the tube inlet, the toroidal vortices resulted in periodic waves in the tube at their shedding frequency. At certain subsonic jet flows, the endwall pressure traces indicated the shedding frequency of these toroidal vortices superimposed on the tube resonance frequency $f \simeq a/4L$. As the nozzle pressure was increased beyond $R > 1{\cdot}9$, the nozzle flow became underexpanded and resulted in the formation of diamond shock cells (shadowgraphs B and C of figure 5*a*). For slightly underexpanded nozzle flows, toroidal vortices could also be seen in the outer part of the jet shear layer. For nozzle pressure ratios $1{\cdot}9 < R \lesssim 3{\cdot}10$, the resonance tube was influenced by the various shock cells. Shadowgraph pictures B and C in figure 5(*a*) clearly indicated more than one shock cell in the jet flow between the nozzle and the tube.

At a nozzle pressure ratio $R = 3{\cdot}16$, the jet flow began to oscillate in the second jet regurgitant mode. Shadowgraph D in figure 5(*b*), from top downwards, represents the series of jet flow shadowgraphs with increasing time during the jet regurgitant mode cycle. In photograph $D1$, the jet flow was in the filling phase of the jet regurgitant mode. Most of the jet flow entered the tube. $D2$ shows the end of the filling phase. The jet flow then switched to the tube efflux phase, which resulted in the formation of an interface between the nozzle jet flow and the tube jet flow. As the outflow phase developed, this interface moved toward the nozzle and resulted in strengthening of the second shock in the nozzle jet flow (photographs $D2$–$D5$). The first shock cell in the nozzle jet flow was not much disturbed as the resonance tube went through a cycle of the second jet regurgitant mode. With increasing time, the tube jet flow weakened and the jet flow between the nozzle and the tube switched suddenly back to the filling phase (figure 5*b*, $D1$). This sequence of behaviour in the jet flow occurred at the resonance tube fundamental frequency $f \simeq a/4L$.

Similar resonance tube behaviour was observed in the sequence of shadowgraph pictures E in figure 5(*b*) at a nozzle pressure ratio of $R = 3{\cdot}73$ for which the resonance tube flow was in the second jet regurgitant mode.

As the pressure was increased further, the resonance tube flow went into the first jet regurgitant mode. These two regurgitant modes associated with the first and second free-jet shock cells were separated by a small range of pressure ratio at which the resonance tube operated in the second jet screech mode. Shadowgraphs F, G, H and I of figures 5(*b*, *c*) represent the sequence of shadowgraph pictures of the jet flow in the first jet regurgitant mode at the higher nozzle pressure ratios indicated. For example, at a pressure ratio of $R = 4{\cdot}91$ (shadowgraph H), the jet flow was initially in the filling phase of the tube ($H1$). After completion of the filling phase, the tube jet flow began. This resulted in the formation of an interface between the nozzle jet and the tube jet flows. With increasing time, this interface moved from the tube inlet toward the nozzle (figure 5*b*, $H2$–$H4$). $H4$–$H6$ represent the jet in the outflow phase. Two normal shock waves on either side of the interface are evident indicating the two jet flows to be supersonic. These shock waves were moving in the opposite direction with respect to the local gas flows. Some of the shadowgraphs in figure 5 were exposed twice and thus showed the jet flow at two instances in a jet regurgitant mode cycle, e.g. $F6$, $G6$, $H5$ and $H6$, etc. As compared to D and E, where the tube flow was in the second jet regurgitant mode, the interaction of the nozzle jet and the tube jet flows was much stronger in the first jet regurgitant mode (F, G, H and I). The stronger shock

waves inside the tube and consequently the higher endwall gas temperatures which resulted will be discussed in § 6.

(ii) *Flow inside tube at $s/d = 3$.* Instant shadowgraphs indicating the tube flow as well as the jet flow between the nozzle exit and the tube inlet for the 35·6 cm tube with spacing $s/d = 3$ are shown in figure 6 (plate 5). These shadowgraphs were taken by exposing two negative films simultaneously which left a line mark on printing and is visible in all the shadowgraphs in figure 6 around the centre of the resonance tube. These pictures were studied along with the sequence of jet flow pictures shown in figure 5. Figures 6*A* and *B* represent the resonance tube in the jet instability mode where toroidal vortices were shed in the jet flow from the nozzle exit, resulting in the generation of a train of very weak shock waves inside the tube at the shedding frequency of these vortices. For slightly underexpanded jet flows (figure 6*C* and *D*), these toroidal vortices could be seen in the jet along with multiple shock cells. Under these flow conditions, the tube was operated in the screech mode by these diamond shock cells at relatively high frequencies as compared to the fundamental tube resonance frequency. Multiple weak wavefronts were generated inside the tube. With increasing pressure, the jet flow began to oscillate in the second jet regurgitant mode. The flows in figure 6*E* and *F* represent the tube flow in the outflow phase of the jet regurgitant mode. The first and second shocks, along with the interface in the jet flow between the nozzle exit and the tube inlet, can be seen (figure 6*F*). No shock waves of significant strength occurred inside the tube flow in the outflow phase (figures 6*D–F*).

Flows in figure 6*G*, *H*, *I*, *J* and *K* represent the resonance tube flow in various phases of the first jet regurgitant mode. A large amount of fine-scale turbulence close to the tube inlet was observed during the inflow phase as seen in figure 6*G*. This turbulent fluid motion is believed to have been caused by the interaction of the impinging nozzle jet flow with the tube inlet. This jet inflow resulted in the formation of an incident shock wave followed by a contact surface. This incident shock wave can be seen travelling toward the endwall in figure 6*G* and resulted in heating the tube gas by dissipative processes across it. The contact surface travelled toward the endwall (behind the incident shock) and divided the tube gas and the nozzle jet flow. The incident shock wave reflected from the endwall and on interaction with the contact surface (which was moving towards the endwall) resulted in strong turbulent mixing. This phase of the jet regurgitant mode is shown in figure 6*H*. The reflected wave is not visible in figure 6*H*, though the turbulent mixing can easily be seen. The reflected shock wave is probably hidden behind the shadow of the bolt. Figure 6*J* represents a similar flow condition at nozzle pressure ratio $R = 4{\cdot}91$ and clearly indicates the reflected shock wave along with the turbulent mixing caused by the interaction of this wave with the contact surface. As the reflected shock wave moved away from this plane of interaction, the flow behind the reflected wave was less turbulent. These shadowgraphs (figures 6*H* and *J*), showing large, fine-scale turbulent fluid motion on collision of the contact surface with the reflected shock wave, strongly suggest that large periodic mixing and exchange of mass between cold nozzle jet flow and the oscillating hot tube flow occur during the inflow phase. The instant shadowgraph in figure 6*I* represents the tube flow at a nozzle pressure ratio $R_s = 4{\cdot}33$, in the outflow phase of the jet regurgitant mode. The interaction of the nozzle and the tube jet flows with the interface in between is evident. The flow inside the tube in this

part of the cycle was relatively free of fine-scale turbulence and of shock waves since only expansion waves existed. These did not result in any abrupt changes in flow and consequently did not have any strong shadow effect. At nozzle pressure $R = 5{\cdot}82$, the flow in figure 6*K* represents the beginning of the inflow phase. One can see an incident shock wave which was travelling towards the endwall of the tube. As expected, the tube flow in front of this incident shock wave was free of turbulence.

The sequences of shadowgraphs in figures 5 and 6 were not taken at high enough nozzle pressure ratios R to operate the resonance tube with spacing $s/d = 3$ discussed above in the jet screech mode. The following results shed some light on this mode of resonance operation.

(iii) *Flow between nozzle exit and tube inlet at* $s/d = 1{\cdot}5$. A sequence of shadowgraph pictures for the 35·6 cm resonance tube with spacing $s/d = 1{\cdot}5$ is shown in figure 7 (plates 6, 7 and 8). Like the shadowgraphs in figure 6, these pictures were taken randomly and have been arranged in sequence of increasing time (from the top downwards) of a typical resonance tube cycle. These shadowgraphs show the jet flow along with the flow close to the inlet of the resonance tube. At a nozzle pressure ratio $R < 1{\cdot}9$ (photographs *A* in figure 7 (*a*)), the resonance tube was in the jet instability mode. No large pressure fluctuations at the endwall of the tube occurred in this mode of operation. As the jet flow became slightly underexpanded with $R = 2{\cdot}04$ (photographs *B* of figure 7*a*), the tube was in the jet screech mode of operation due to the influence of the multiple diamond shocks. Both in the jet instability mode and in the slightly underexpanded jet screech mode of operation, weak compression wave fronts were observed along the resonance tube. Shadowgraphs *C* in figure 7 (*a*) represent the flow in the second jet screech mode (§ 8). These figures clearly show a normal shock wave which always stood in front of the tube inlet. The first shock location and its strength did not change with time in this case.

At a nozzle pressure ratio of $R = 2{\cdot}60$ (photographs *D* in figure 7*b*), the jet flow went into the regurgitant mode associated with the first shock cell. *D*1–*D*3 represent with increasing time the inflow phase of the jet regurgitant mode. There was considerable turbulent fluid motion close to the tube inlet in this phase of the regurgitant mode when most of the nozzle jet flow entered the tube. The jet structure in the filling phase was quite independent of the presence of the tube. *D*4 represents the outflow phase. In this phase, as one would expect, no mixing close to the tube inlet occurred. As the tube jet flow gathered strength, an interface was formed which moved from the tube inlet toward the nozzle exit. This resulted in strengthening of the nozzle shock, which became almost a normal shock as it moved toward the nozzle exit (*D*5 and *D*6).

The sequence of shadowgraphs *E* in figure 7 (*b*), at nozzle pressure $R = 3{\cdot}47$, shows the jet regurgitant mode similar to that of *D*. In these pictures, the interface can be seen very clearly in the outflow phase of the regurgitant mode (*E*5 and *E*6). As the pressure was increased beyond $R \gtrsim 3{\cdot}9$, the jet flow switched to the jet screech mode for the 35·6 cm resonance tube with $s/d = 1{\cdot}5$.

Typical shadowgraphs of the jet flow in the screech mode at a nozzle pressure $R = 3{\cdot}96$ are shown in figure 7 (*b*) (series *F*). As pointed out earlier, a normal shock which oscillated at high frequency as compared to the fundamental resonance tube frequency for this tube (which was approximately 250 Hz) always stood in front of the resonance tube inlet. The screech frequency was approximately 4 kHz and increased

slightly with increasing nozzle pressure ratio. By noting the flow close to the resonance tube inlet, it is apparent that very little nozzle jet flow entered the tube compared to the inflow phase of the jet regurgitant mode. As will be discussed subsequently, weak shock waves (as compared to the jet regurgitant mode) were observed at the oscillation frequency of this normal shock, which always stood in front of the tube. The jet flows in figure 7 (*c*) represent the jet screech mode at higher nozzle pressure ratios R.

(iv) *Flow inside tube at* $s/d = 1{\cdot}5$. Shadowgraphs of the resonance tube and jet flows at various nozzle pressures of the 35·6 cm resonance tube with spacing $s/d = 1{\cdot}5$ are shown in figure 8 (plate 9). In figure 8*A* the subsonic jet flow and the train of waves inside the tube were at the frequency of the toroidal vortices shed from the nozzle exit. At a pressure ratio $R = 2{\cdot}04$, the tube was under the influence of the second diamond shock. With increased nozzle pressure, as discussed previously, the jet flow switched to the jet regurgitant mode. Figure 8*C* represents the resonance tube flow in the inflow phase of the jet regurgitant mode. Considerable turbulence can be seen close to the inlet of the tube. Figure 8*D* at $R = 3{\cdot}16$ represents the outflow phase of the regurgitant mode and does not show large irregular motion close to the inlet of the tube.

For a nozzle pressure ratio $\geqslant 3{\cdot}96$, the resonance tube went into the jet screech mode. This resulted in the formation of an almost normal shock which in turn resulted in a train of weak shock waves inside the tube at the frequency of its oscillations. The flows in figures 8*E*, *F*, *G*, *H* and *I* represent the jet screech condition at higher nozzle pressure ratios. These pictures clearly show multiple wavefronts travelling into and out of the tube. Very little of the nozzle jet flow entered the tube in this mode of operation as compared to that in the jet regurgitant mode in the inflow phase *C*.

5. Endwall pressure measurements

Endwall pressure measurements were made over a large range of spacings s/d, nozzle pressure ratios, and for different tube lengths with piezoelectric pressure transducers. A study of these traces along with the corresponding endwall gas temperature traces allowed further insight into the heating mechanism of the tube gas.

Typical endwall pressure traces for the 35·6 cm resonance tube with spacing $s/d = 3$ at various nozzle pressures are shown in figure 9 (plate 10). In comparing the endwall pressure traces at different nozzle pressure ratios, it should be noted that the vertical and horizontal scales in figure 9 are not identical for all the traces. Endwall pressure traces for subsonic jet flows (see traces in figure 9 at pressure ratios $R = 1{\cdot}23$ and 1·50) show weak periodic signals. As pointed out above, these waves in the tube were caused by the interaction of the toroidal vortices with the resonance tube inlet. These weak pressure oscillations in the tube did not result in heating the gas near the endwall. For certain nozzle flow and tube configurations, the non-dimensional frequency of the toroidal vortices was observed to be superimposed on the endwall pressure signal at the fundamental resonance tube frequency, i.e. $f \simeq a/4L$.

As the nozzle pressure ratio was increased beyond $R > 1{\cdot}9$, the jet flow was underexpanded and, as discussed above (§ 4), resulted in the formation of diamond shock wave cells. At low underexpansion nozzle pressure ratios, the tube with spacing $s/d = 3$ was excited in the screech mode by these multiple shock wave cells. Typical endwall

pressure traces for the jet screech mode excited by multiple shock cells are shown in figure 9 at nozzle pressure ratios $R = 2{\cdot}04$ and $2{\cdot}60$. At a nozzle pressure ratio $R \simeq 3{\cdot}16$, the tube flow went into the second jet regurgitant mode (see the corresponding jet flow between the nozzle exit and the tube mouth, shadowgraphs D in figure 5*b*). One clearly sees the shock wave followed by compression waves in figure 9 at $R = 3{\cdot}16$. This wave was formed during the inflow phase of the jet regurgitant mode. As this compression wavefront reached the resonance tube inlet after reflexion from the endwall (thus completing the inflow phase), it resulted in generation of an expansion wavefront. This wavefront travelled toward the endwall and resulted in the initiation of the jet outflow phase. During the time it took for this expansion wavefront to reach the endwall, as is clear from the endwall pressure trace, the pressure remained constant. As the expansion wavefront arrived at the endwall, the endwall pressure decreased and reached the lowest pressure in this cycle of regurgitant mode operation. The outflow phase was completed as the expansion fan reached the resonance tube inlet after reflexion from the endwall. The tube flow then switched to the jet inflow phase and resulted in a sudden pressure jump across the incident shock followed by compression waves. This cycle took place at the fundamental resonance frequency of the tube. The endwall pressure trace at $R = 3{\cdot}73$ in figure 9 also represents the resonance tube flow in the jet regurgitant mode excited by the second shock wave cell.

At a nozzle pressure ratio of $R = 4{\cdot}33$, the resonance tube began to oscillate in the first jet regurgitant mode. The endwall pressure trace at $R = 4{\cdot}33$ indicated a much stronger normal shock wave in the tube compared to the trace at $R = 3{\cdot}16$ or $3{\cdot}73$ in figure 9. This is expected because the first shock wave cell is much stronger than the second shock wave cell; there is a stronger inflow phase when the tube is placed under the influence of the first shock cell as compared to the second one. The corresponding gas temperature in the vicinity of the endwall was higher when the tube was in the first jet regurgitant mode as compared to the second. As the nozzle pressure was increased further (e.g. $R = 4{\cdot}91$ and $5{\cdot}49$), the endwall pressure traces showed a reduction in the strength of the shock wave in the compression phase of the jet regurgitant mode and resulted in a reduction of the corresponding endwall gas temperatures.

The endwall pressure traces in the jet screech mode of tube operation showed small-amplitude, high-frequency (as compared to jet regurgitant mode) periodic oscillations and will be discussed in detail in § 8 (cf. figure 7). As will be discussed in § 6, sudden changes in the endwall gas temperature occurred when the resonance tube flow switched from the jet regurgitant to the jet screech mode. This study showed that these high-frequency endwall oscillations were caused by the oscillating normal shock which always existed between the resonance tube inlet and the nozzle exit in the screech mode. Results presented in § 6 showed that very high endwall gas temperatures were obtained when the resonance tubes were tuned to these high-frequency shock wave oscillations in the jet screech mode.

It was also observed that in the jet regurgitant mode of resonance tube operation, the strength of the endwall pressure traces (after the initial transient period) were independent of time; i.e. the strength of the shock waves inside the tube did not change with time.

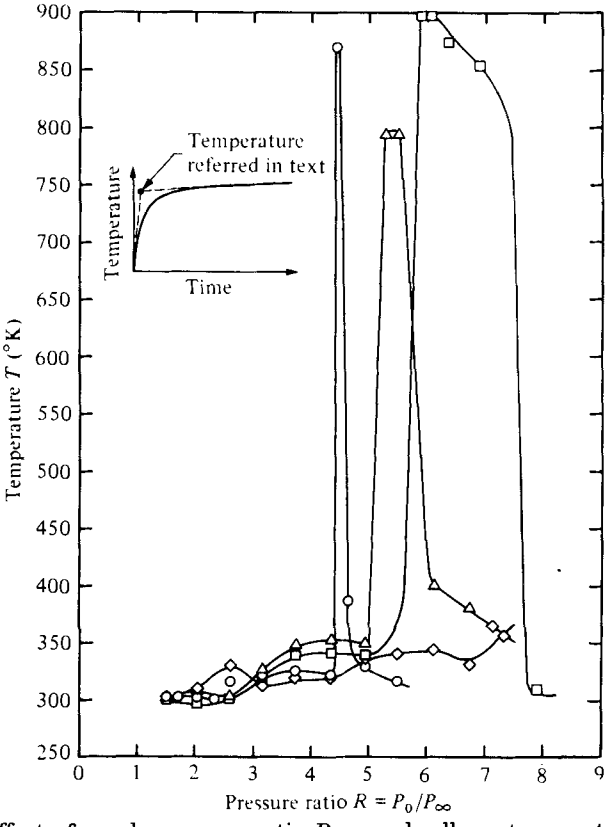

FIGURE 10. Effect of nozzle pressure ratio R on endwall gas temperature for 7·6 cm tube. ○, s/d = 1·5; △, s/d = 1·75; □, s/d = 2·00; ◇, s/d = 3·00.

6. Temperature measurements in resonance tubes

Endwall gas temperatures for various resonance tube flow conditions for which the endwall pressure traces as well as the flow visualization discussed above were obtained with a thermocouple whose output was recorded on an oscilloscope. The temperatures referred to in the following section were defined as shown in the insert in figure 10. Most of the temperatures referred to below, therefore, were recorded in less than 100 ms. But the actual rise time of the endwall gas temperature is believed to be shorter than the recorded rise time. This was mainly attributed to thermal inertia of the thermocouple junction and conduction losses to the endwall of the resonance tube. When the highest heating in the resonance tube was attained (approximately 900 °K) the tube charred. Thus, the highest temperature referred to is only up to the time that tube failure occurred, which was approximately 50 ms or less in these experiments.

The effect of upstream nozzle pressure ratio R on the endwall gas temperature for the 7·6 cm resonance tube with spacings s/d = 1·5, 1·75, 2, and 3 are shown in figure 10. For subsonic flow (pressure ratio $R < 1{\cdot}9$), the jet flow was in the jet instability mode, during which there was little rise in the endwall gas temperature, as indicated in figure 10. For low underexpanded nozzle flows, the flow visualization and endwall pressure traces showed the resonance tube flow in the jet screech mode excited by the

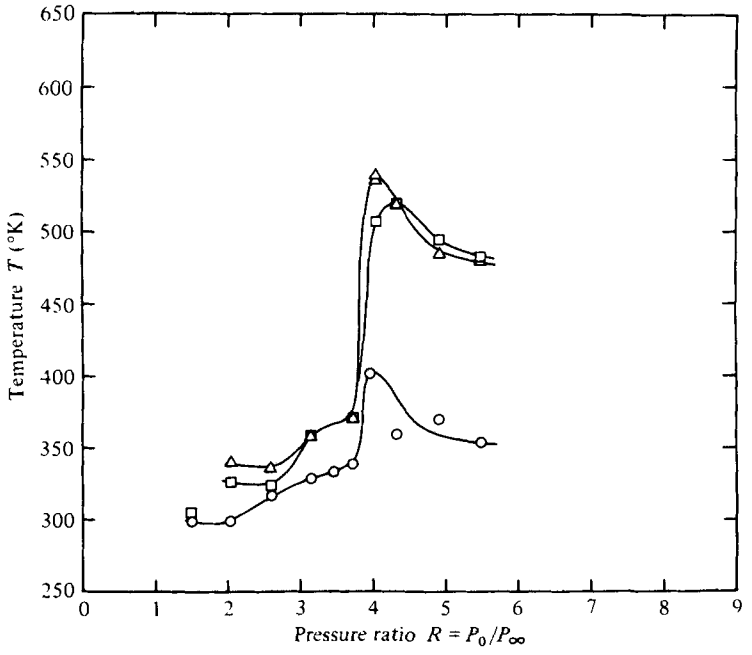

FIGURE 11. Effect of nozzle pressure ratio R on endwall gas temperature for 35·6 cm resonance tube. ○, s/d = 1·5; △, s/d = 3·00; □, s/d = 4·00.

multiple shock cells. This resulted in weak compression waves at the screech frequency and did not result in significant heating of the gas near the endwall.

The resonance tube flow switched to the jet regurgitant mode at a nozzle pressure R of about 2·40 and remained in this mode up to $R \simeq 4{\cdot}35$ for $s/d = 1{\cdot}5$. In the jet regurgitant mode, endwall pressure traces showed oscillations at the fundamental resonance frequency $f \simeq a/4L$, which for this 7·6 cm long tube was approximately 1000 Hz. The compression part of the endwall pressure trace when the resonance tube flow was in the jet regurgitant mode showed no shock waves. Because of the comparatively short tube length, the compression waves generated by the inflow phase of the jet regurgitant mode had no time to coalesce to form shock waves. Consequently, the rise in temperature which occurred through these trains of compression waves was nearly isentropic. As these compression waves were reflected from the tube inlet as expansion waves (at the end of the inflow phase), the endwall tube gas was cooled back to the initial temperature isentropically. No significant heating resulted, therefore, in the regurgitant mode cycle. Since the response time of the thermocouple was 50 ms or less, it was reading a mean temperature in this cycle. The time period of 1 ms for the jet regurgitant mode cycle of the 7·6 cm tube was very small compared to thermocouple response time. For these short tubes, hardly any increase in endwall gas temperature occurred in the jet regurgitant mode as indicated in figure 10.

At a nozzle pressure ratio of about $R \simeq 4{\cdot}35$, the jet tube switched to the jet screech mode. As soon as the tube flow switched to the screech mode, the endwall gas temperature suddenly rose to approximately 870 °K and resulted in the charring of the lucite walls of the resonance tube. As the nozzle pressure was increased a little further, as

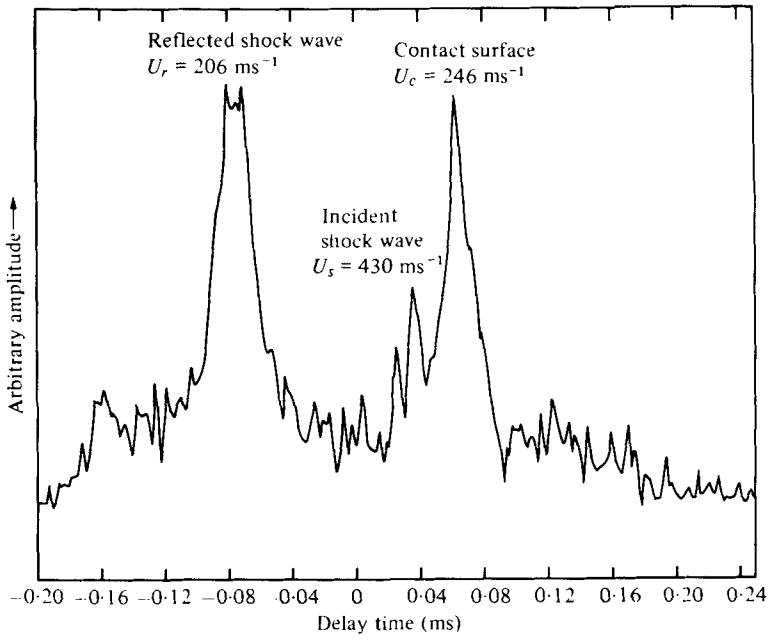

FIGURE 12. Cross-correlation of laser data, 35·6 cm tube, s/d = 3, spacing between laser beams is equal to 1·55 cm.

shown in figure 10, the gas temperature decreased suddenly almost to ambient temperature. This drastic heating and abrupt cooling of the endwall gas with a change in nozzle pressure ratio was also observed by Sprenger (1954). These effects will be discussed in detail in § 8.

The general behaviour of the endwall gas temperature for other spacings s/d with nozzle pressure ratio for the 7·6 cm resonance tube was identical with that explained above for s/d = 1·5. The two main features were that with increased spacing the switch from jet regurgitant to jet screech mode occurred at high nozzle pressures. The range of pressure over which this intense heating occurred (with tube failure) increased as shown in figure 10. For a spacing s/d = 3, no intense heating zone was observed over the range of nozzle pressures tested because the tube flow remained in the jet regurgitant mode.

The results in figure 11 represent the endwall gas temperature in the 35·6 cm resonance tube with spacings s/d = 1·5, 3, and 4 at various nozzle pressures. As compared to shorter tubes, considerably higher endwall gas temperatures were obtained in the jet regurgitant mode. This was due to the increased tube length, which allowed the compression waves to coalesce and form the shock wavefront. These resulted in the generation of heat by dissipative processes across the shock waves formed in the tube (increased entropy), leading to an increase in the endwall gas temperature. For spacing s/d = 1·5, as the tube flow switched to screech mode at nozzle pressure $R \simeq 4{\cdot}3$, there was a small drop in endwall gas temperature. Under identical flow and tube spacing, it should be recalled that the 7·6 cm tube showed a temperature of about 870 °K in figure 10. For larger spacings s/d = 3 and 4, higher endwall gas temperatures were obtained in the jet regurgitant mode as compared to

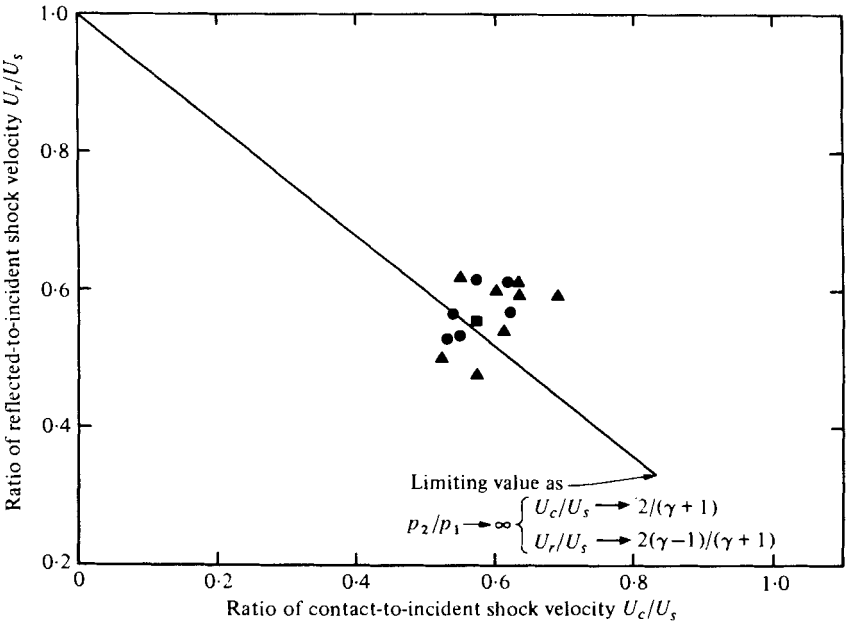

FIGURE 13. Comparison of experimentally measured wave shock velocity with predicted results in regurgitant mode for 35·6 cm resonance tube operation. Laser data: ●, $s/d = 3$; ▲, $s/d = 4$. Pressure transducer data: ■, $s/d = 3$.

spacing $s/d = 1{\cdot}5$. Thus it was concluded that the length of the tube played a key role in endwall gas temperature both in the jet screech and the jet regurgitant modes.

7. Experimental and theoretical wave speeds in resonance tubes

In the jet regurgitant mode of resonance tube operation, shock wave and contact surface velocities were measured using two laser beams. These velocities were determined from the beam spacing and the delay time. A typical cross-correlation of the data is shown in figure 12 along with the incident shock U_s, reflected shock U_r, and contact surface U_c, velocities for the 35·6 cm resonance tube with spacing $s/d = 3$ and pressure ratio $R = 4{\cdot}04$. In this case, the spacing between the centres of the two beams was 1·55 cm.

A comparison between experimental and predicted velocities for the jet regurgitant operating mode for spacings $s/d = 3$ and 4 is shown in figure 13. The solid curve in figure 13 is the theoretical prediction for shock wave reflexion from the endwall of the tube,

$$\frac{U_r}{U_s} = 1 - \left(\frac{3-\gamma}{2}\right)\frac{U_c}{U_s}. \tag{1}$$

As shown in this figure, reasonably good agreement with theory was obtained.

Theoretical reflexion shock wave and contact surface velocities can also be expressed in terms of the pressure ratio P_2/P_1 across the incident shock wave, i.e. $(U_r/U_s)\,(P_2/P_1, \gamma)$ and $(U_c/U_s)\,(P_2/P_1, \gamma)$, for example see Landau & Lifshitz (1959). It was not possible, however, to measure the absolute pressure levels with the piezoelectric pressure transducers accurately because of gas heating near the endwall. The output of the

quartz transducers drifted with temperature. By placing pressure transducers on the sidewall of the resonance tube, the pressure increases across the incident (P_2-P_1) and reflected (P_3-P_2) shock waves were measured, and the pressure ratio P_2/P_1 was determined from the following relation for shock wave reflexion from the endwall of the tube (Shapiro 1954)

$$\frac{P_3-P_2}{P_2-P_1}=\frac{\frac{2\gamma}{\gamma+1}\left(\frac{P_2}{P_1}\right)}{1+\frac{\gamma-1}{\gamma+1}\left(\frac{P_2}{P_1}\right)}. \tag{2}$$

The pressure increases across the incident and reflected shock waves are not affected by transducer ouptut drift with temperature, and absolute levels of pressure P_1, P_2 and P_3 were thus determined.

Figure 14 (plate 10) shows the typical sidewall as well as the endwall pressure traces. These traces were taken for the 35·6 cm tube with spacing $s/d = 3$ when the tube was operating in the jet regurgitant mode. The top trace in this figure was at the endwall, whereas the middle and bottom traces were at $x/d = 12$ and 6, respectively. The middle trace, which was close to the endwall, clearly indicates the incident and the reflected shock wave strengths. The pressure increases across the incident and the reflected waves were read from this trace to determine the absolute levels of the pressures as well as the wave velocities inside the tube.

A typical value for the ratio of pressure increase across the incident and across the reflected shock waves was $(P_3-P_1)/(P_2-P_1) = 3{\cdot}53$ for the 35·6 cm resonance tube with spacing $s/d = 3$. This corresponds to a pressure ratio across the incident shock $P_2/P_1 \simeq 3{\cdot}40$. The Mach number of the incident shock wave M_s was found to be 1·75. Also, the ratio of the contact surface velocity to the incident shock velocity $U_c/U_s \simeq 0{\cdot}56$, and the ratio of the reflected shock wave velocity to the incident shock wave velocity $U_r/U_s \simeq 0{\cdot}55$. These results are indicated on figure 13 and the agreement with the predicted result is good.

In the above case, the pressure jump across the incident shock wave was $P_2-P_1 \simeq 7{\cdot}58\ \mathrm{N/cm^2}$ (11·0 psi) and the pressure ratio across this wave P_2/P_1 was 3·40. The absolute pressures were $P_1 \simeq 3{\cdot}03\ \mathrm{N/cm^2}$ (4·4 psia) in front of the incident shock wave, $P_2 \simeq 10{\cdot}75\ \mathrm{N/cm^2}$ (15·6 psia) behind the incident shock wave, and $P_3 \simeq 29{\cdot}8\ \mathrm{N/cm^2}$ (43·2 psia) behind the reflected shock wave.

Of note is that, in the jet regurgitant mode, pressures below atmospheric were observed before the inflow phase was initiated. Behind the incident shock wave, the pressures were close to the atmospheric pressure of $9{\cdot}86\ \mathrm{N/cm^2}$ (14·3 psia).

8. Criteria for intense heating of resonance tubes

One of the most intriguing aspects of resonance tube performance in this investigation was when the tube flow switched from a regurgitant mode to a jet screech mode. To emphasize the results, the key features of this change in resonance tube mode of operation are summarized below:

(i) With increasing nozzle pressure the change of jet flow from regurgitant to screech mode resulted in drastic changes in endwall temperature as shown in figures 10 and 11. For the 7·6 cm resonance tube there was intense heating when this change in

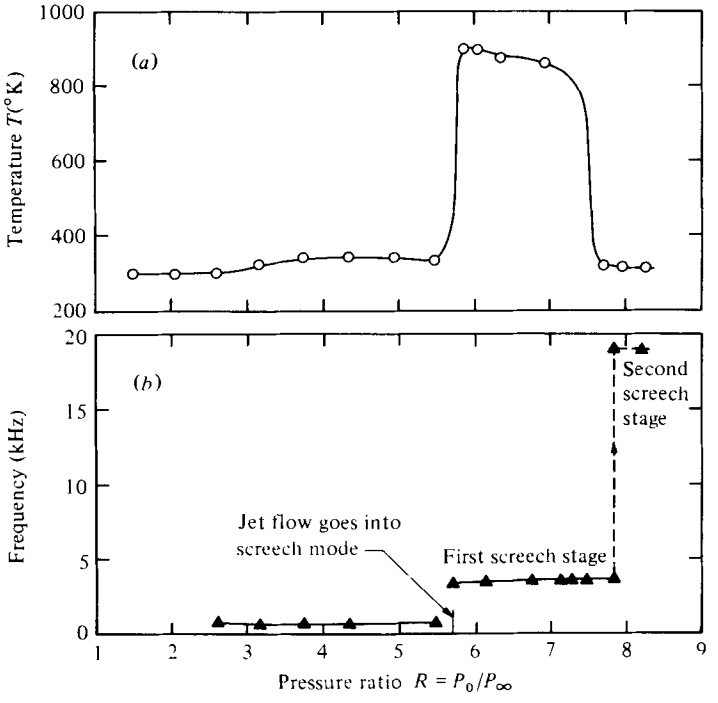

FIGURE 15. Endwall gas temperatures in various modes of 7·6 cm resonance tube operation with spacing $s/d = 2$.

mode occurred; however, for the 35·6 cm tube there was a drop in endwall gas temperature. On the other hand, when the pressure was increased further for the 7·6 cm resonance tube in jet screech mode, a sudden drop in endwall gas temperature was observed.

(ii) As the tube flow went into the jet screech mode, a normal shock appeared in front of the resonance tube inlet. This normal shock wave oscillated about its mean position at high frequency. These high-frequency shock oscillations generated relatively weak waves inside the resonance tube as compared to those in the jet regurgitant mode.

(iii) In comparison to the inflow phase of the jet regurgitant mode, only a small amount of nozzle jet mass flow entered the tube in the screech mode. The normal shock wave in front of the tube inlet acted like a 'leaky piston' oscillating at a high frequency.

The cause of the intense heating in the jet screech mode over a range of nozzle pressure ratios is discussed subsequently in this section. An understanding of this mechanism can be helpful in designing a resonance tube system for a particular mode of operation.

The effect of nozzle pressure ratio on endwall gas temperature for the 7·6 cm resonance tube with spacing $s/d = 2$ is shown in figure 15. Also shown on the figure are the corresponding frequencies of the endwall pressure traces. As discussed in § 6 (cf. figure 10), no significant endwall gas heating occurred in the jet regurgitant mode. As the nozzle pressure was increased, in the jet regurgitant mode, the frequency of the endwall pressure trace remained almost constant at the fundamental resonance

frequency of the tube, which for the 7·6 cm tube was approximately 1000 Hz. As the resonance tube switched to the jet screech mode at a nozzle pressure ratio of 5·75, the endwall pressure signal indicated a jet screech frequency of about 3500 Hz. This was accompanied by a sudden jump in the endwall gas temperature to about 900 °K, accompanied by charring of the lucite tube. As the nozzle pressure ratio R was increased above 5·75, the screech frequency increased slowly until a nozzle pressure ratio of 7·85 was reached. The resonance tube flow jumped to a higher stage of jet screech with an endwall pressure signal frequency of 18 kHz. This caused a sudden drop in the endwall gas temperature.

The endwall pressure traces of the jet regurgitant, first and second stages of jet screech mode of operation for the 7·6 cm resonance tube with spacing $s/d = 2$, are shown in figure 16 (plate 12). The endwall pressure trace at a nozzle pressure ratio of 4·91 was at a tube resonance frequency of about 1000 Hz with the tube flow in the jet regurgitant mode. The pressure traces at nozzle pressure ratios of 5·82, 6·74, 7·28 and 7·82 were for the first stage of jet screech mode with a tube oscillation frequency of about 3500 Hz. As compared to the jet regurgitant mode, the amplitude of the waves in the tube was smaller for the first stage of jet screech mode. The intense heating in the first stage of jet screech mode was accompanied by little periodic mass exchange between the oscillating hot tube flow and the cold nozzle jet flow. When the resonance tube flow switched to higher stages of jet screech mode at a pressure ratio of 8·27, the frequency of the waves in the tube increased to approximately 18 kHz. A pronounced reduction in endwall gas temperature was accompanied by the formation of relatively weak waves inside the tube. In comparing the amplitude of endwall pressure traces in the first and second stages of the jet screech mode in figure 16, it should be noted that the vertical scales are not identical.

Figure 17 (plate 13) indicates the jet flow in the regurgitant mode, and first and second stages of screech mode. These pictures have been arranged with increasing time from top down for a typical cycle of tube operation. Set A in figure 17 represents the jet flow in the regurgitant mode for a nozzle pressure ratio of 4·91. Set B in figure 17 represents the flow in the first stage of jet screech mode during which intense heating of the endwall gas occurred; these pictures show a normal shock present constantly in front of the resonance tube. This shock wave oscillated with large amplitude in a cycle about its mean position. These large-amplitude shock oscillations subsided as the resonance tube flow switched to a higher stage of screech mode above a nozzle pressure ratio of 7·85. Typical shadowgraphs of the jet flow in the second stage of screech mode are shown in set C of figure 17. This jet flow configuration did not heat the endwall gas. The shadowgraphs indicated that the sudden drop in endwall gas temperature was accompanied by very small amplitude oscillations of the normal shock in the jet flow between the nozzle exit and the tube inlet. This resulted in comparatively weak waves inside the tube; e.g. see the pressure trace at nozzle pressure ratio of 8·27 in figure 16.

The amplitude of this normal shock between the nozzle exit and tube inlet in the first and in the second stages of the jet screech mode of the 7·6 cm tube with $s/d = 2$ was determined relative to the free-jet shock location $(X_s/s)_{\text{free jet}}$ and the Mach disc $(X_m/d)_{\text{free jet}}$ as a function of nozzle pressure ratio. The experimental results in figure 18 for nozzle pressure ratios less than 5·75 pertain to the regurgitant mode. The shock location in the inflow phase of the jet regurgitant mode was close to the free-

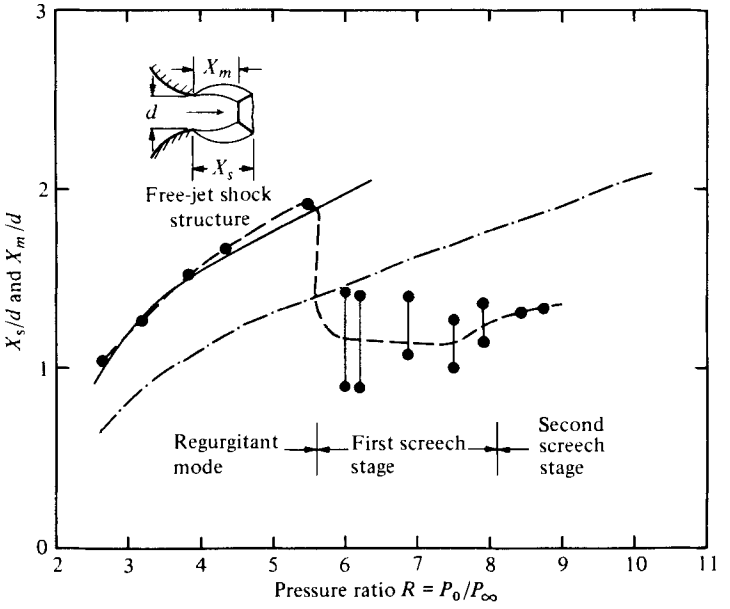

FIGURE 18. Shock wave location in various modes of 7·6 cm resonance tube operation with spacing $s/d = 2$. ●, experimental shock wave location; ——, first free-jet shock (X_s/d); –·–·, free-jet Mach disc (X_m/d).

jet shock location. At a nozzle pressure ratio of 5·8, when $(X_s/d)_{\text{free jet}} \simeq s/d$, the tube flow switched to the first stage of jet screech mode. The large amplitude of the oscillating jet shock wave which produced an intense heating condition has been shown in figure 18 by joining the minimum shock location $(X_s/d)_{\min}$ and the maximum shock location $(X_s/d)_{\max}$ by a vertical line. This amplitude remained on the order of 10–25 % of the tube spacing s/d until a nozzle pressure ratio of 7·85 was reached. The jet flow shock wave then began to oscillate at a frequency $f \simeq 18$ kHz. The high-frequency jet flow shock oscillation had a very small amplitude and did not cause heating of the endwall gas.

The intense heating of the endwall gas in the first stage of screech mode resulted in charring of the lucite tube. On critical analysis of these tubes it was concluded that large-amplitude oscillations of the shock wave in the jet flow were accompanied by the presence of locally heated node points indicating the presence of standing waves inside the tube.

This intense heating is characterized as follows:

(i) Resonance tube in jet screech mode with jet flow shock oscillation frequency in tune with one of the resonance frequencies of the tube.

(ii) Large-amplitude oscillations of this normal shock between the nozzle exit and the tube inlet occur with amplitude as large as 15–20 % of the nozzle exit diameter.

(iii) As compared to the inflow phase of the jet regurgitant mode, a small fraction of the nozzle jet flow enters the tube. Consequently, little mass exchange results during each cycle of the jet screech mode.

(iv) Most of the dissipative heat energy generated by irreversible processes across the compression wavefronts is trapped between the node points of the tuned intense

heating resonance tube system in the jet screech mode. Because of reduced mass exchange between the cold nozzle jet flow and the oscillating hot tube flow in each jet screech mode cycle (which is believed to be the principal source of heat removal from resonance tubes), intense heating of the gas near the endwall results. This is due to cumulative heat addition to the trapped endwall gas by dissipative processes across these high-frequency compression waves. These originate from the screeching shock wave in the jet flow acting like a 'leaky' driving piston.

(v) As the resonance tube flows go out of resonance with the oscillating shock wave, e.g. with higher stages of jet screech mode such as shown in figure 15, no standing waves appear inside the tube and insignificant heating of the endwall gas occurs.

9. Discussion

According to Hartmann (1931), high intensity sound vibrations are generated when the resonance tube is placed in the region where the pressure in the jet is rising, i.e. the spatial zone of instability. The present measurements show that the regurgitant and screech modes are separated when this zone of spatial instability for the free jet begins, i.e. free-jet shock location X_s, is equal to the spacing s, for a given jet flow condition. The results in figure 3 can be used to design a given resonance tube system to operate either in the jet regurgitant mode or in the jet screech mode. Results of the present experiments indicate that the criterion for operating a given resonance tube system in the jet screech mode (i.e. to have the corresponding free-jet shock location $X_s/d_{\text{free jet}}$ greater than the spacing s/d) works well until the shear layer behind the Mach disc begins to interact with the resonance tube inlet. It is believed that the tube inlet configuration also plays a role when a switch from regurgitant to screech mode occurs, e.g. the ratio of free-jet Mach disc diameter to tube inlet diameter. This interaction of the shear layer between the oscillating shock wave and resonance tube inlet at higher nozzle pressure ratios may have resulted in the departure of the experiments from the above criterion in separating the regions of jet regurgitant and screech modes (figure 3). Further experiments investigating the influence of the tube inlet configuration on various resonance tube modes are needed.

In the jet screech mode, the shock wave in the jet flow oscillated in various bands of frequencies, as has previously been observed (Hartmann 1931; Brun & Boucher 1957). In each band of jet flow screech operation, the oscillation frequency of the shock wave decreased with an increase of spacing for a given nozzle pressure, and increased with increasing nozzle pressure with a fixed spacing. This behaviour of the jet flow shock wave oscillation in the jet screech mode indicates that these oscillations may be driven by the shear layer located behind this shock and the resonance tube inlet. Such shear flows are inherently unstable and are known to sustain periodic oscillations (Sarohia 1976). Additional studies of this shear flow between the oscillating shock and the resonance tube inlet in the jet screech mode would shed more light on these self-sustained oscillations of the shock wave.

Shadowgraphs in the inflow phase of the jet regurgitant mode showed that most of the jet flow entered the tube. This resulted in formation of an almost normal shock, followed by a contact surface. This contact surface separated the oscillating hot tube gas from the entering nozzle jet flow. Shadowgraphs showed a strong mixing and large

turbulent motion when the contact surface collided with the reflected shock wave. It is believed that the contact surface due to rushing nozzle jet flow (during the inflow phase of the jet regurgitant mode) may not be plane. Owing to non-uniform contact surface, large periodic turbulent mixing may result between the nozzle-jet cold gas and the oscillating hot gas inside the resonance tube (figures 6*H* and *J*). Therefore, most of the heat generated in the jet regurgitant mode, which occurs mainly by dissipative processes across the shock waves formed in the tube in the inflow phase of the regurgitant mode cycle, is carried away periodically by the tube jet flow during the outflow phase of the regurgitant mode. This source of heat removal in the jet regurgitant mode has not been taken into account in the theoretical procedures of Shapiro (1960) and of Wilson & Resler (1959). This may be the reason why the predicted endwall temperatures of the tube gas estimated to be on the order of $2(\gamma+1)$ times the average gas temperature by Shapiro (1960) are much higher than the measured ones in the jet regurgitant mode previously discussed with regard to figures 10 and 11.

This work presents the results of one phase of research carried out at Jet Propulsion Laboratory, California Institute of Technology, under Contract NAS 7–100, sponsored by the National Aeronautics and Space Administration. It is a pleasure to thank P. F. Massier for his helpful suggestions and encouragement throughout this research. We are indebted to Dr J. E. Roschke and Dr S. P. Parthasarathy for their support, interest and assistance during the course of this investigation. The authors are grateful to Wayne Bixler, Scotty Slover, Stanley Kikkert and Don Feller for fabricating the hardware for the present experiments.

REFERENCES

Brocher, E., Maresca, D. & Bournay, M. H. 1970 *J. Fluid Mech.* **43**, 369.

Brocher, E. & Maresca, C. 1973 *Int. J. Heat Mass Transfer* **16**, 529. (N.A.S.A. Tech. Transl. F **14**, 796).

Brun, E. & Boucher, R. M. G. 1957 *J. Acoust. Soc. Am.* **29**, 573.

Hartmann, J. 1931 *Phil. Mag.* **11**, 926.

Landau, L. D. & Lifshitz, E. M. 1959 *Fluid Mechanics*, p. 365. Pergamon.

Lloyd, E. C. 1958 *Nat. Bureau Standards Rep.* 6443.

Marchese, P. 1974 N.A.S.A.-CR-2418.

Mørch, K. A. 1964 *J. Fluid Mech.* **20**, 141.

Rozenburg, L. D. 1969 *Source of High-Intensity Ultrasound.* Plenum Press. (Translated from Russian.)

Sarohia, V. 1977 *A.I.A.A. J.* **15**, 984.

Shapiro, A. A. 1954 *The Dynamics and Thermodynamics of Compressible Fluid Flow*, vol. II. Ronald Press.

Shapiro, A. H. 1960 *J. Aero. Sci.* **27**, 66.

Sprenger, H. S. 1954 Über Thermische Effekte bei Rezonanzrohrem. *Mitteilungen aus dem Institut für Aerodynamik an der E.T.H., Zürich*, Nr. 21, 18. (AERE lib/trans. 687).

Stabinsky, L. 1973 *Rockwell International Rep.* 9403.

Thompson, A. 1960 Ph.D. thesis, Massachusetts Institute of Technology.

Vrebalovich, T. 1962 *Jet Prop. Lab., Tech. Rep.* no. 32–378.

Westley, R. & Woolley, J. H. 1968 *Proc. AFOSR–UTIAS Symp. Aerodyn. Noise, Toronto, Canada.*

Wilson, J. & Resler, E. J. 1959 *J. Aero. Sci.* **26**, 461.

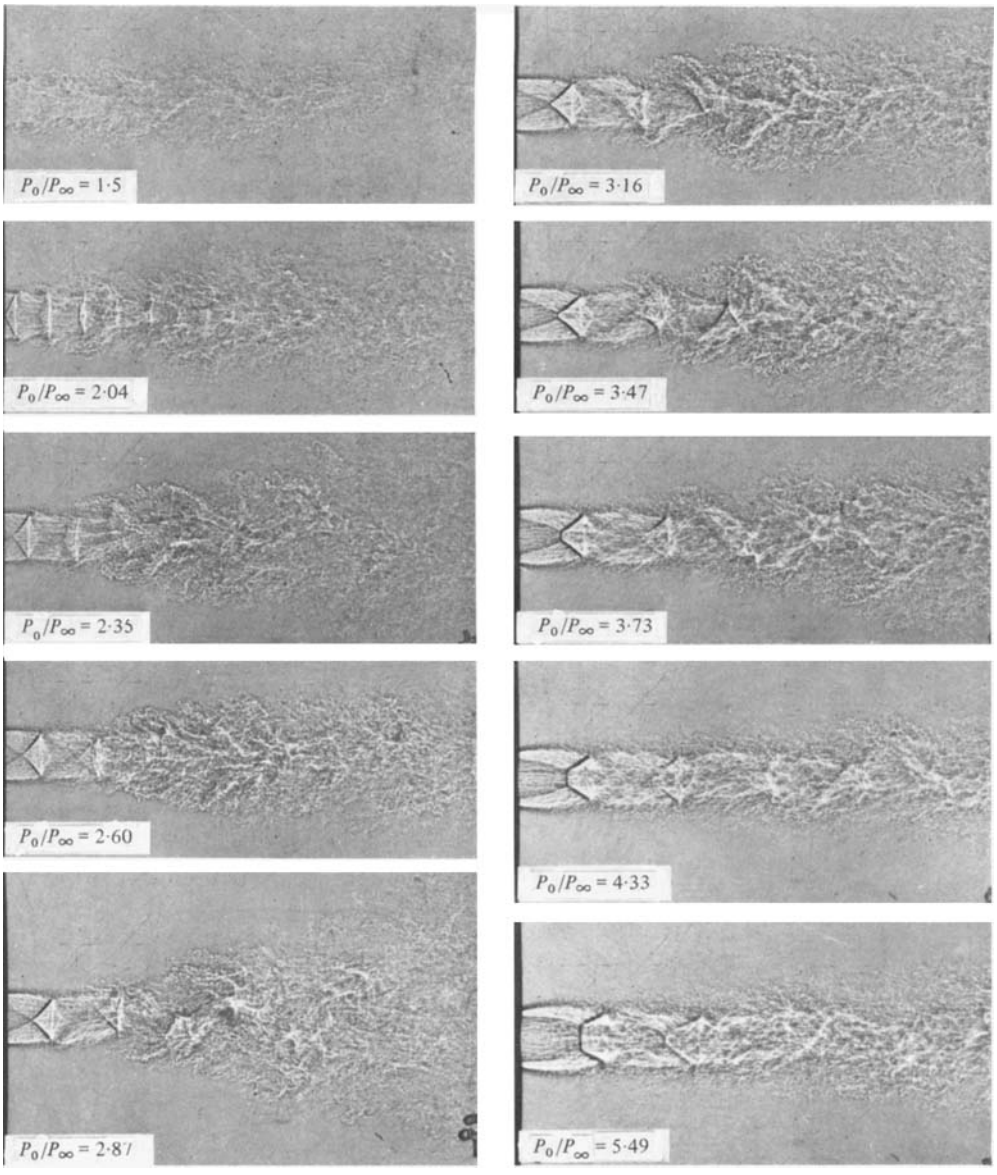

FIGURE 4. Free-jet shadowgraph pictures at different nozzle pressure ratios R.

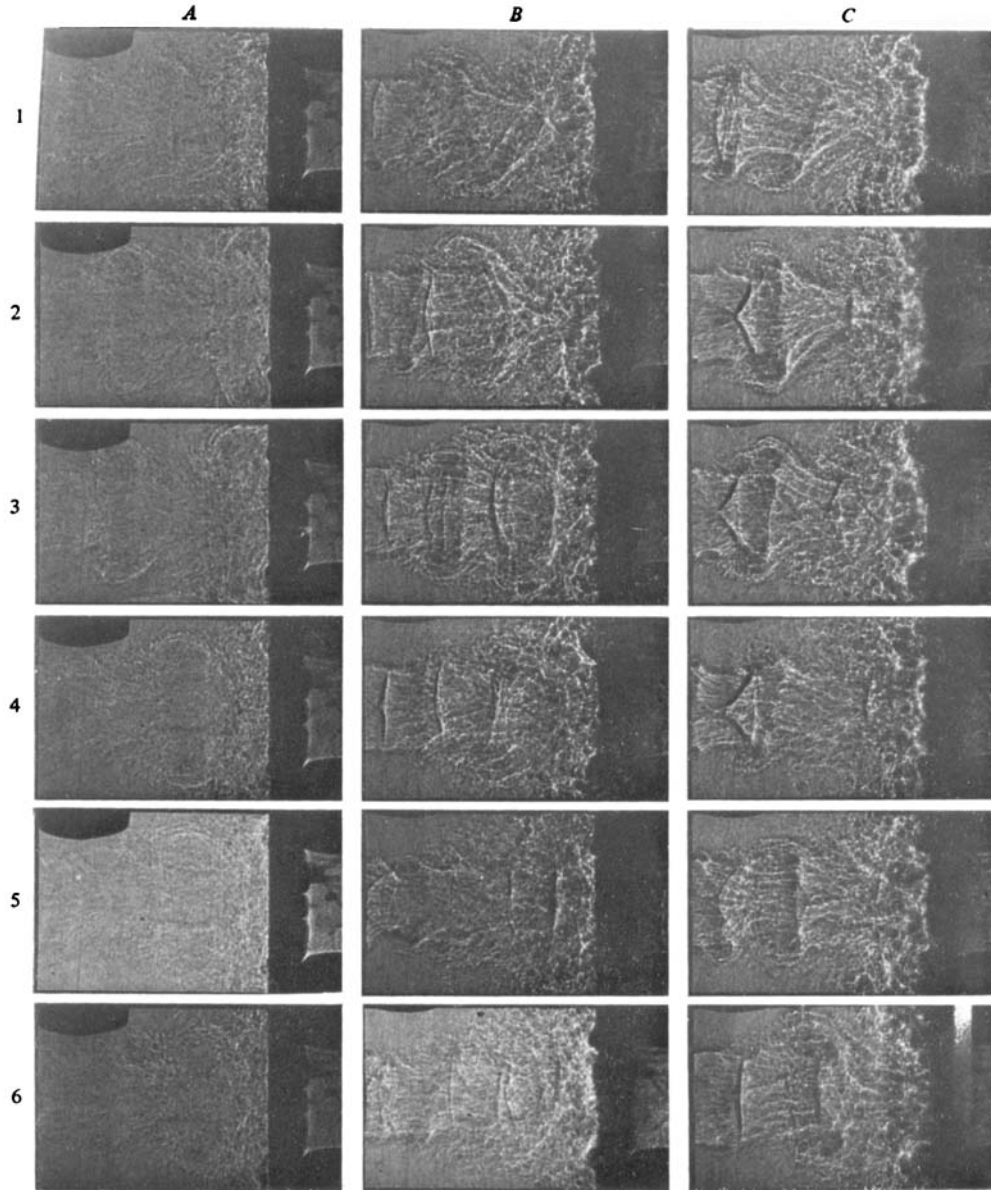

FIGURE 5. Sequence of jet flow shadowgraph pictures of 35·6 cm resonance tube at different nozzle pressure ratios R with spacing $s/d = 3$. *A*, $P_0/P_\infty = 1{\cdot}23$; *B*, 2·04; *C*, 2·60; *D*, 3·16; *E*, 3·73; *F*, 4·04; *G*, 4·33; *H*, 4·91; *I*, 5·49.

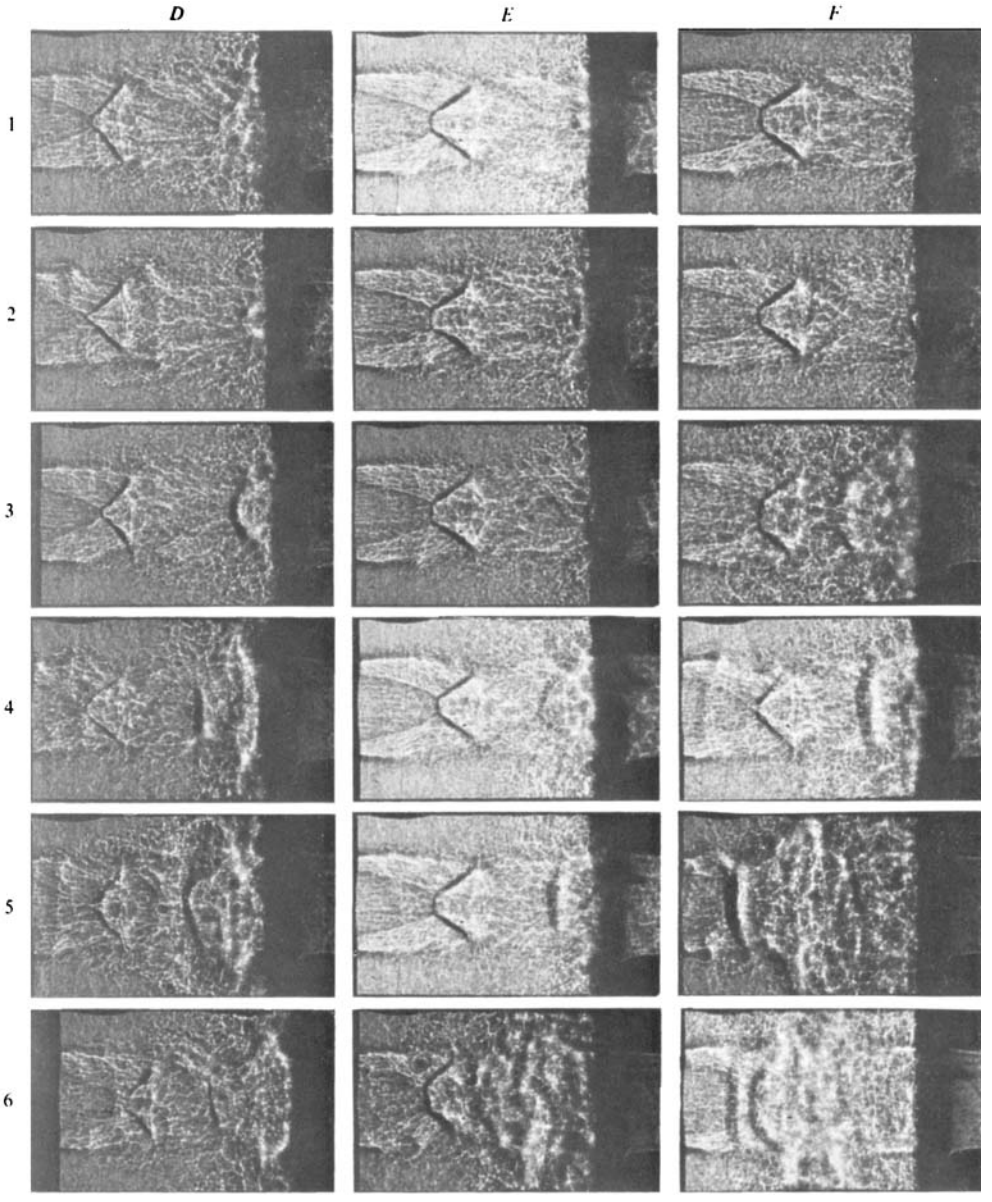

FIGURE 5. For legend see plate 2.

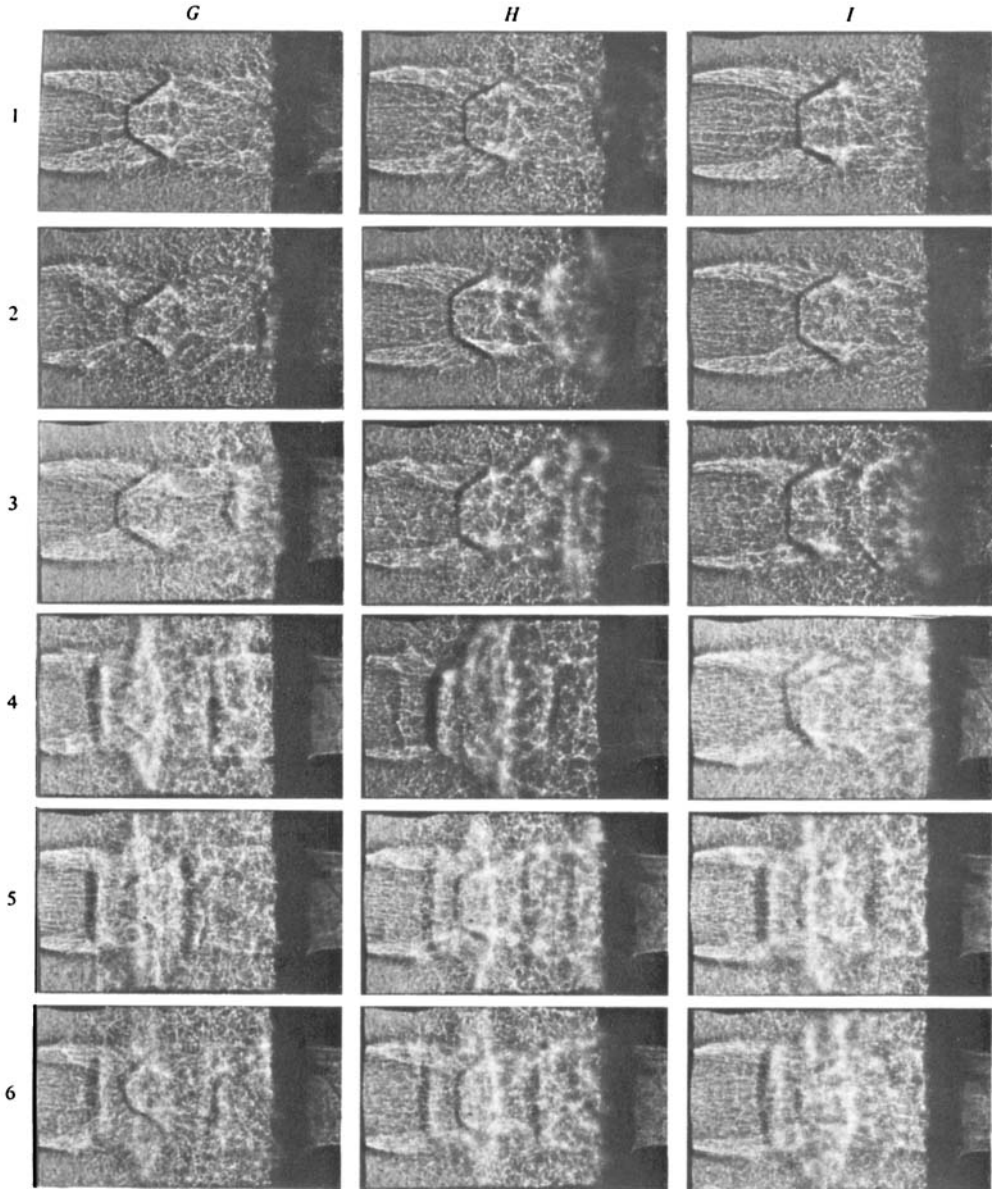

FIGURE 5. For legend see plate 2.

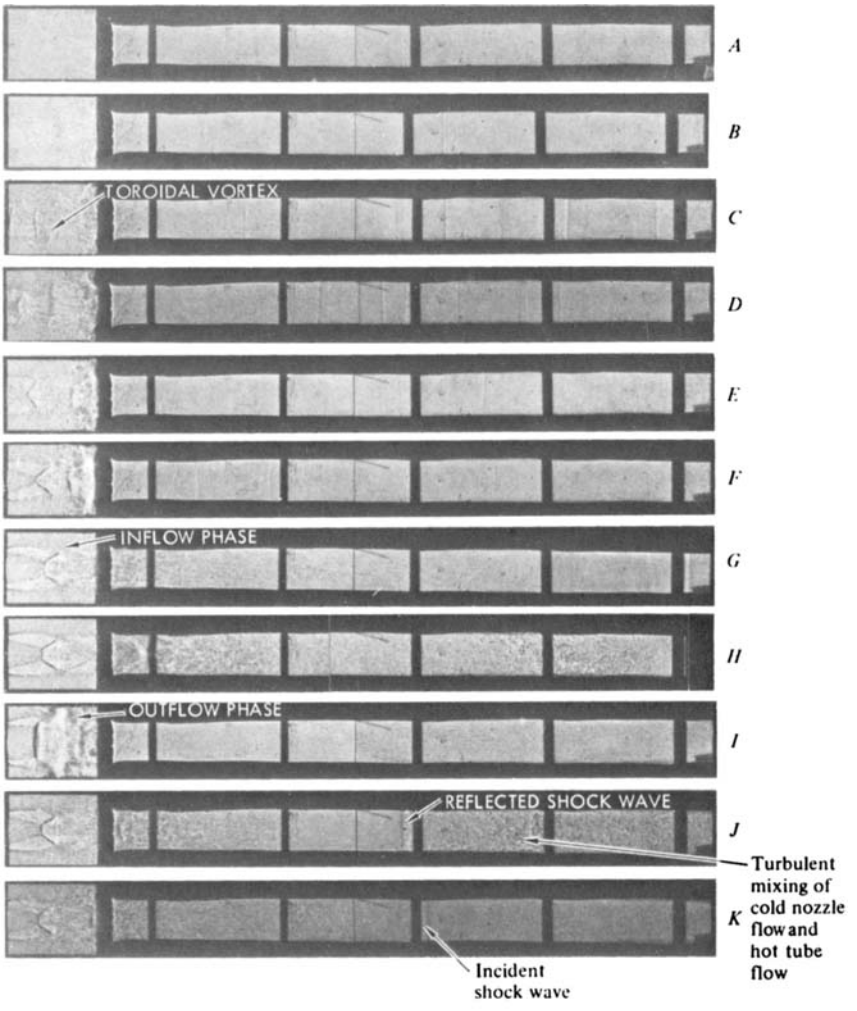

FIGURE 6. Sequence of shadowgraph pictures of 35·6 cm resonance tube at different nozzle pressure ratios R with spacing $s/d = 3$. A, $P_0/P_\infty = 1{\cdot}23$; B, 1·50, C, 2·04; D, 2·60; E, 3·16; F, 3·73; G, 4·04; H, 4·04; I, 4·33; J, 4·91; K, 5·82.

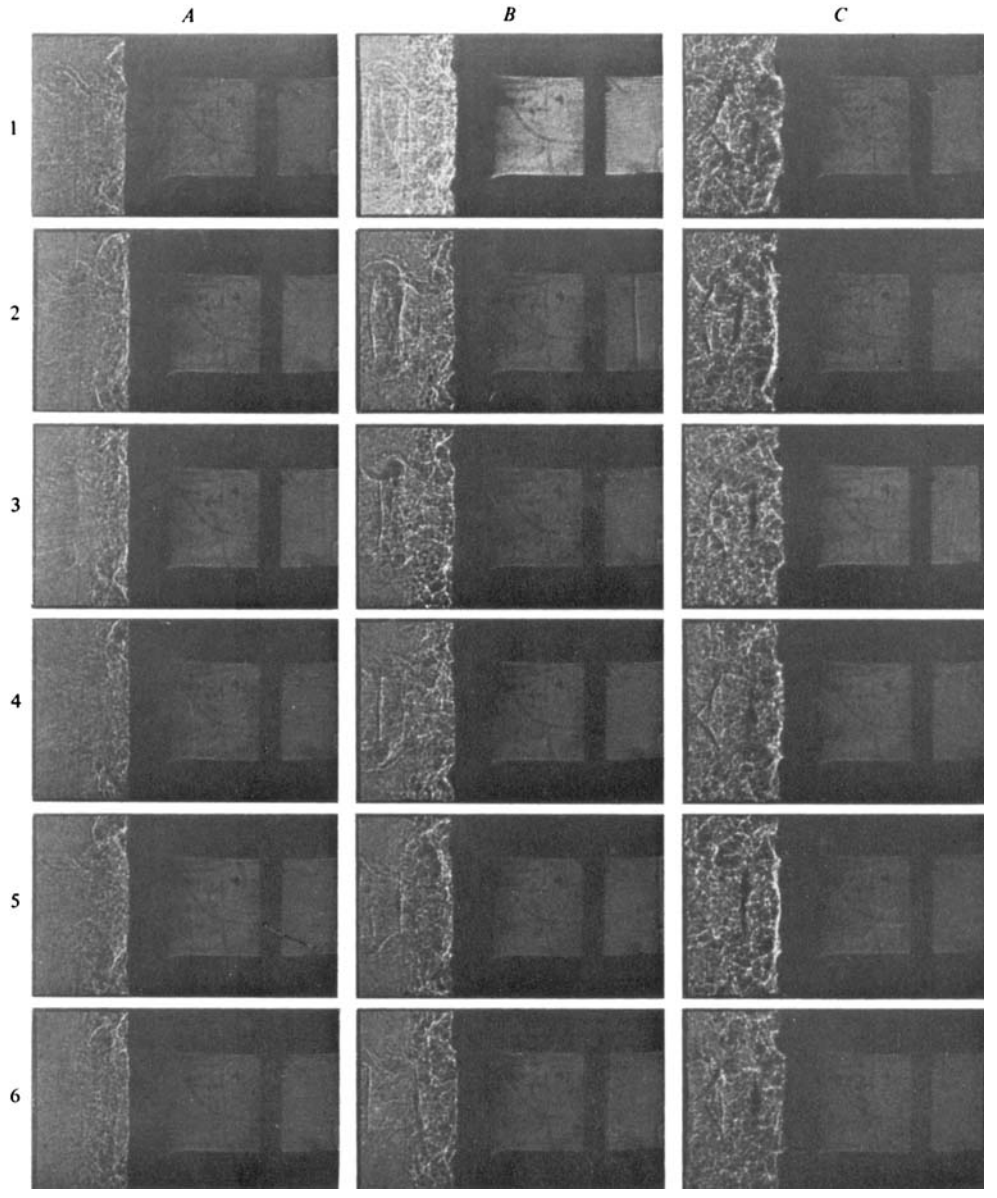

FIGURE 7. Sequence of jet-flow shadowgraph pictures of 25·6 cm resonance tube at different nozzle pressure ratios R with $s/d = 1{\cdot}5$. *A*, $P_0/P_\infty = 1{\cdot}5$; *B*, 2·04; *C*, 2·35; *D*, 2·60; *E*, 3·47; *F*, 3·96; *G*, 4·33; *H*, 4·91; *I*, 5·49.

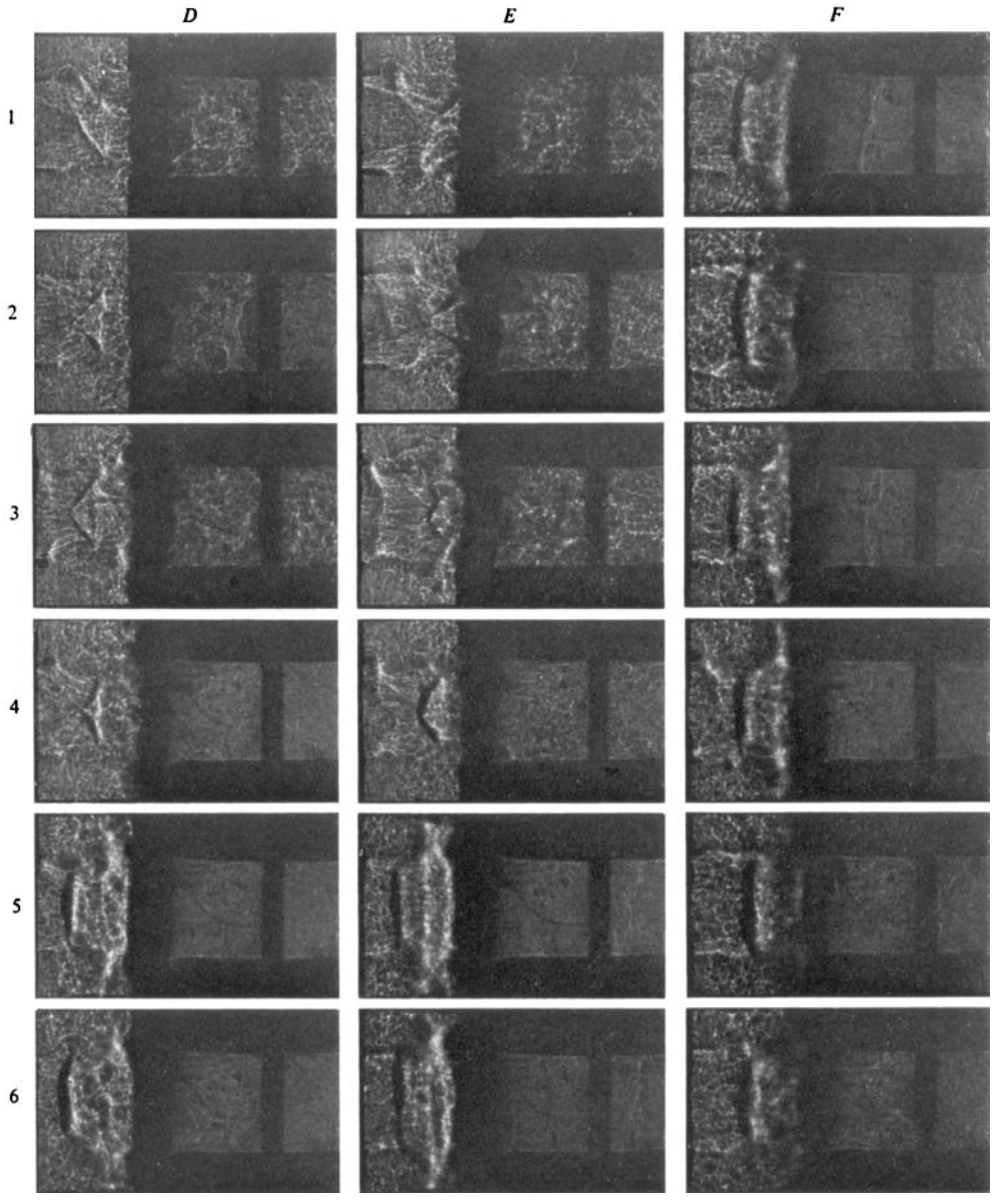

FIGURE 7. For legend see plate 6.

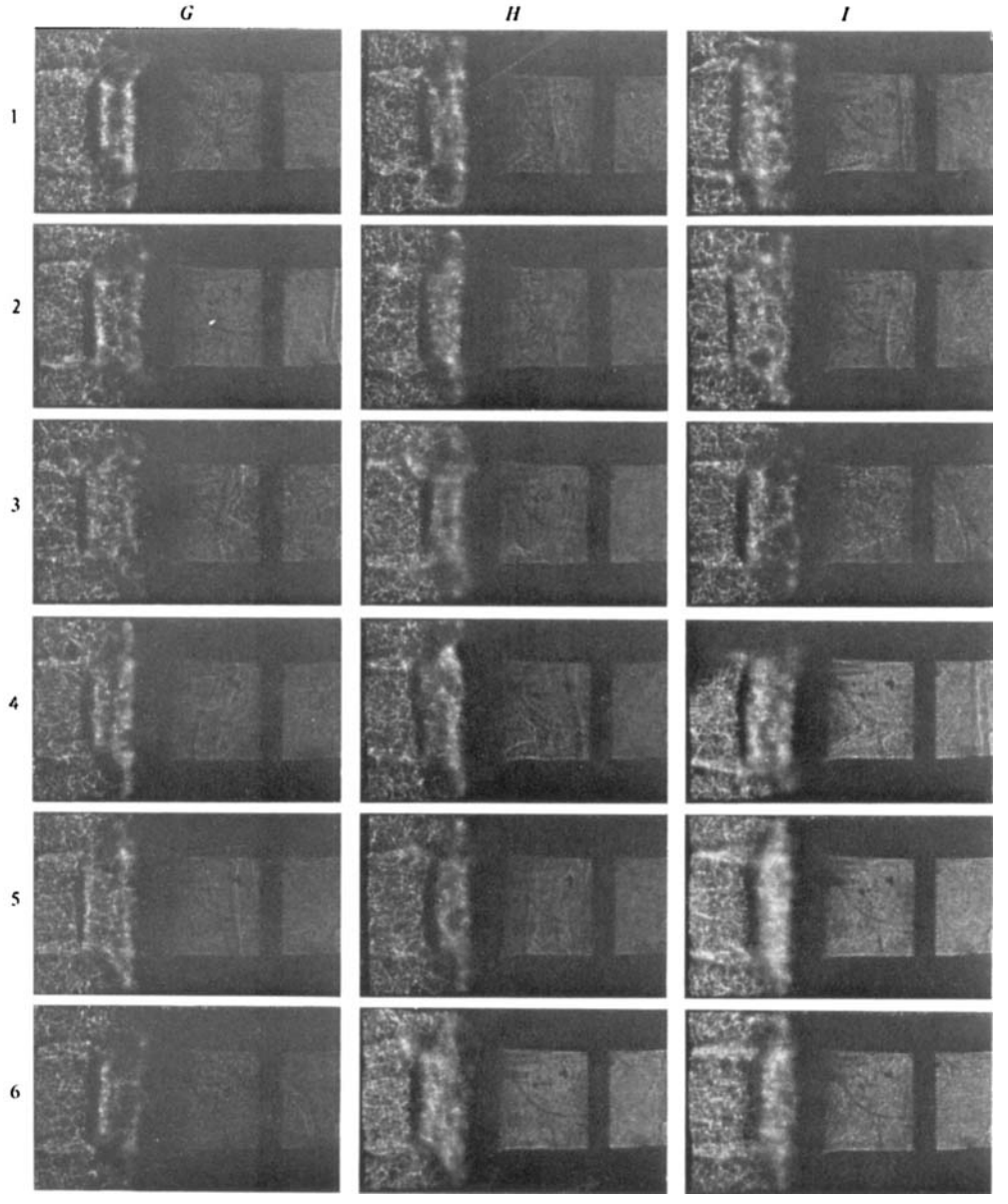

FIGURE 7. For legend see plate 6.

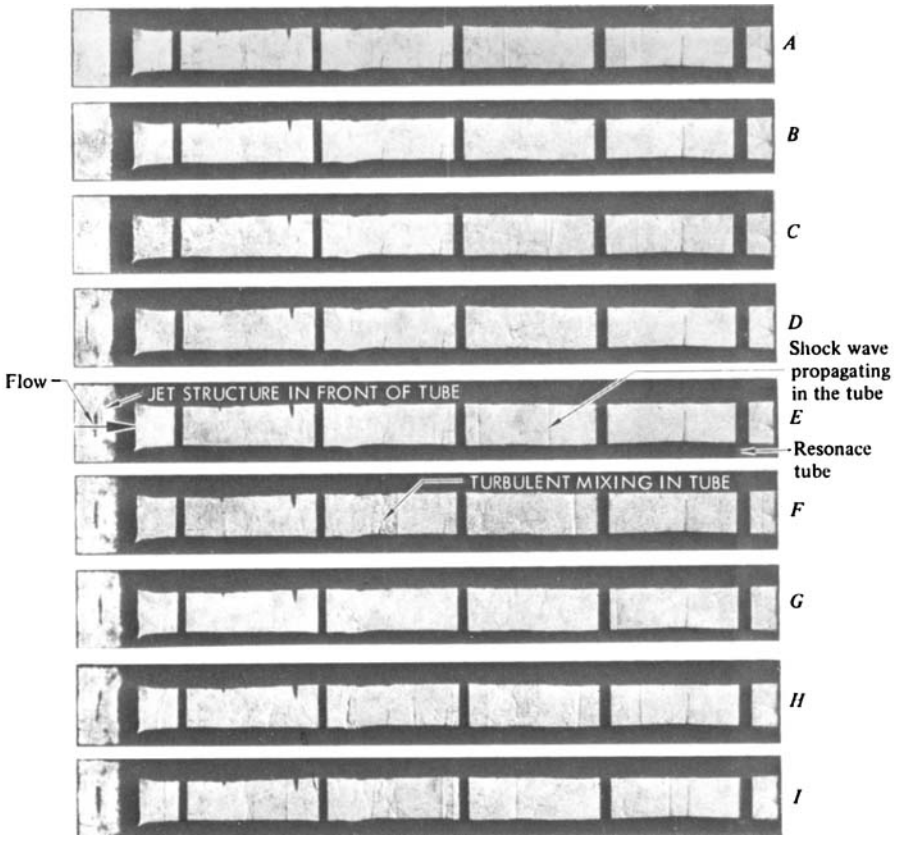

FIGURE 8. Sequence of shadowgraph pictures of 35·6 cm resonance tube at different nozzle pressure ratios R with spacing $s/d = 1{\cdot}5$. A, $P_0/P_\infty = 1{\cdot}5$; B, 2·04; C, 2·60; D, 3·16; E, 3·73; F, 4·04; G, 4·33; H, 4·91; I, 5·49. A, jet instability mode; B–E, jet regurgitant mode; F–I, jet screech mode.

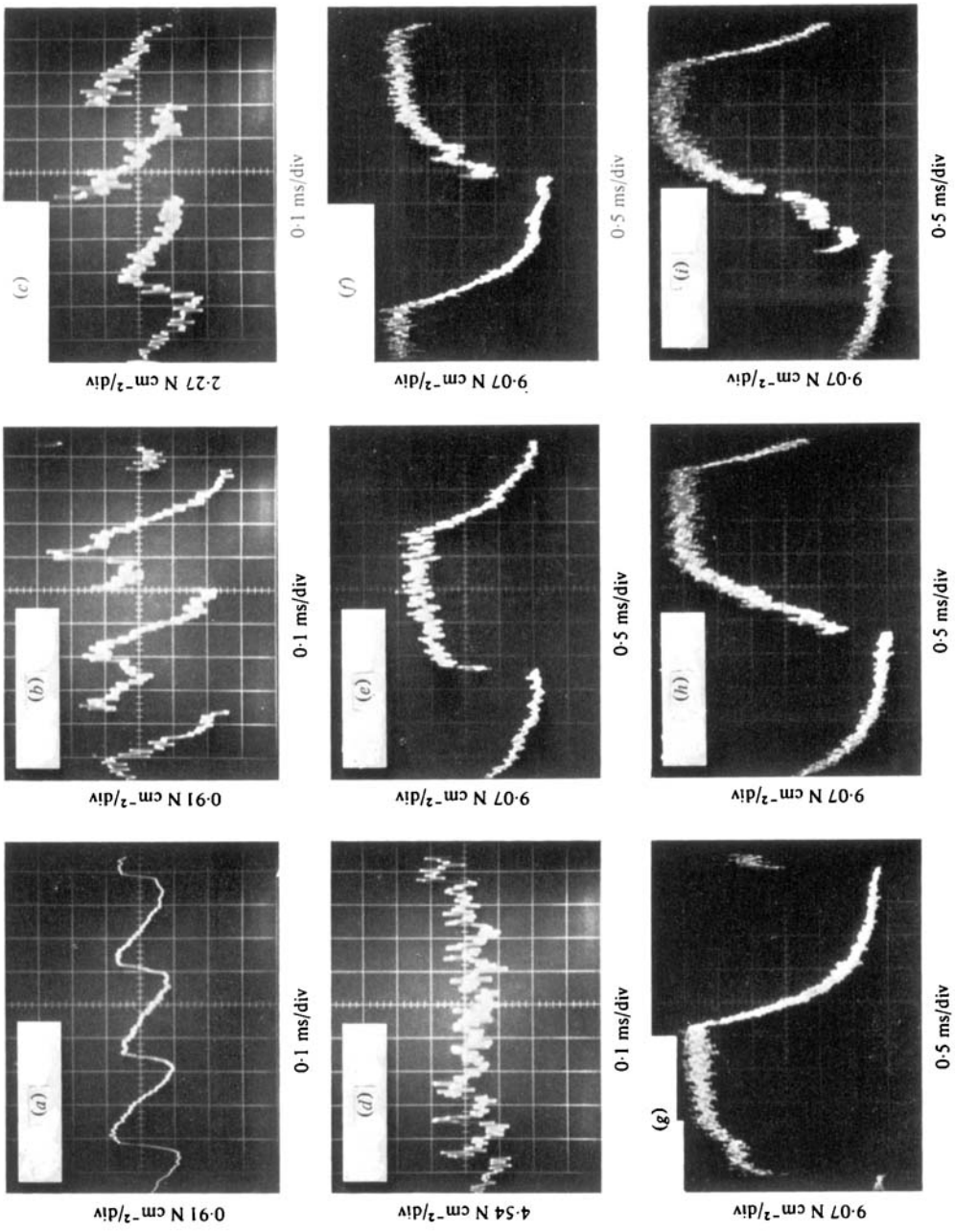

FIGURE 9. Typical endwall pressure traces of 35·6 cm resonance tube at different nozzle pressure ratios R with spacing s/d = 3. (*a*) P_0/P_∞ = 1·23; (*b*) 1·50; (*c*) 2·04; (*d*) 2·60; (*e*) 3·16; (*f*) 3·73; (*g*) 4·33; (*h*) 4·91; (*i*) 5·49.

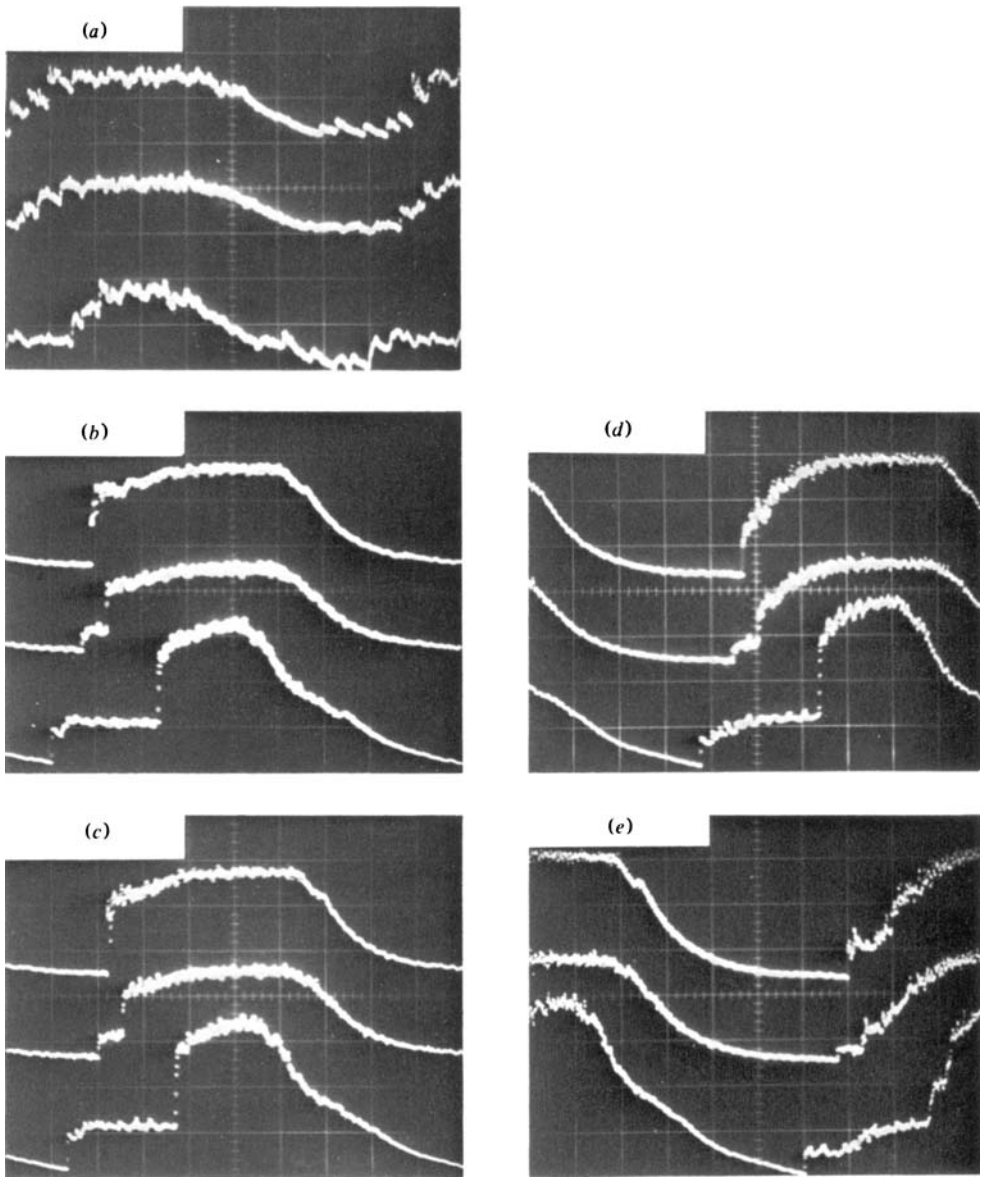

FIGURE 14. Typical pressure traces of 35·6 cm resonance tube at $x/d = 6$, $x/d = 12$, and endwall for different nozzle pressure ratios R with spacing $s/d = 3$. (*a*) $P_0/P_\infty = 3{\cdot}16$; (*b*) 4·04; (*c*) 4·33; (*d*) 4·91; (*e*) 6·49. Horizontal scale 0·5 ms/div.; vertical scale: top traces (endwall) 22·68 N cm^{-2}/div.; middle traces ($x/d = 12$) 18·44 N cm^{-2}/div.; bottom traces ($x/d = 6$) 9·07 N cm^{-2}/div.

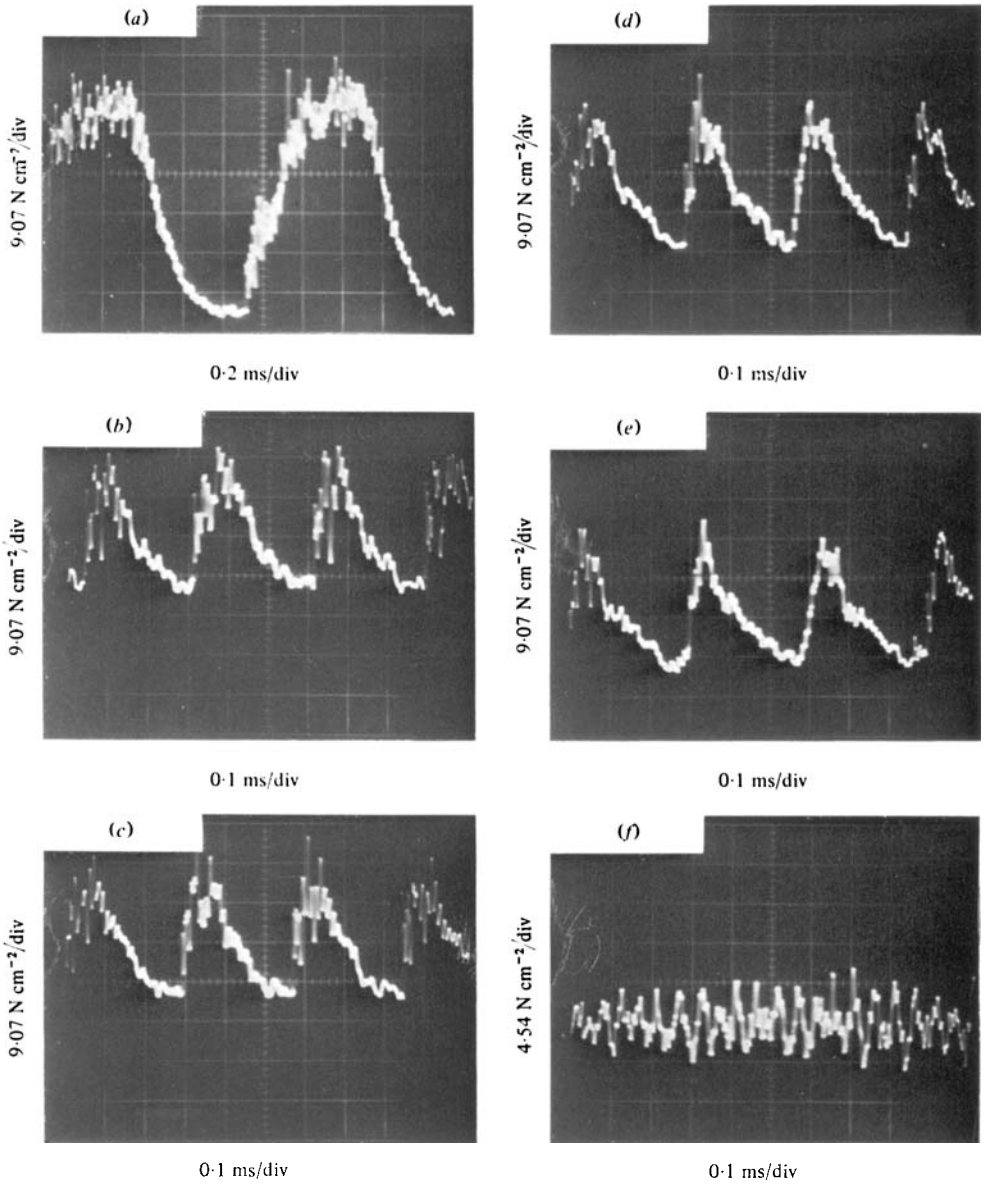

FIGURE 16. Oscilloscope record of pressure at endwall of 7·6 cm resonance tube in different modes of operation with spacing $s/d = 2$. (*a*) $P_0/P_\infty = 4{\cdot}91$; (*b*) 5·82; (*c*) 6·74; (*d*) 7·28; (*e*) 7·82; (*f*) 8·27.

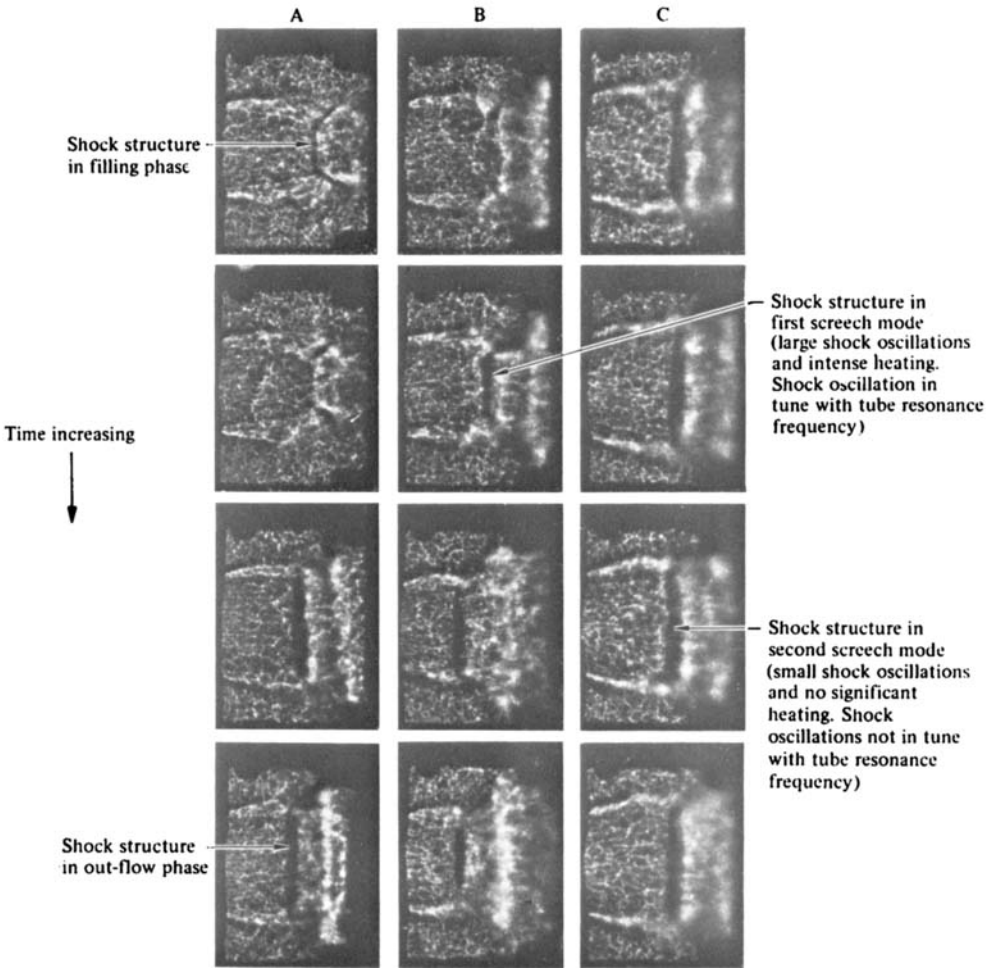

FIGURE 17. Sequence of jet flow shadowgraph pictures of 7·6 cm resonance tube in different modes of operation with spacing $s/d = 2$. *A*, regurgitant mode; *B*, first screech mode; *C*, second screech mode.